

Synthesis, characterization and anti-inflammatory activity evaluation of 1,2,4-triazole and its derivatives as a potential scaffold for the synthesis of drugs against prostaglandin-endoperoxide synthase

Bushra Khan, Abdullah Naiyer, Fareeda Athar, Shakir Ali & Sonu Chand Thakur

To cite this article: Bushra Khan, Abdullah Naiyer, Fareeda Athar, Shakir Ali & Sonu Chand Thakur (2020): Synthesis, characterization and anti-inflammatory activity evaluation of 1,2,4-triazole and its derivatives as a potential scaffold for the synthesis of drugs against prostaglandin-endoperoxide synthase, Journal of Biomolecular Structure and Dynamics, DOI: [10.1080/07391102.2019.1711193](https://doi.org/10.1080/07391102.2019.1711193)

To link to this article: <https://doi.org/10.1080/07391102.2019.1711193>

 View supplementary material 

 Accepted author version posted online: 03 Jan 2020.

 Submit your article to this journal 

 View related articles 

 View Crossmark data 

Synthesis, characterization and anti-inflammatory activity evaluation of 1,2,4-triazole and its derivatives as a potential scaffold for the synthesis of drugs against prostaglandin-endoperoxide synthase

Bushra Khan^{1,#}, Abdullah Naiyer^{1,#}, Fareeda Athar¹, Shakir Ali², Sonu Chand Thakur^{1,*}

¹Centre for Interdisciplinary Research in Basic Sciences, Jamia Millia Islamia, Delhi, India

²Department of Biochemistry, School of Chemical and Life Sciences, Jamia Hamdard, Delhi

³DBT BTISNet Bioinformatics infrastructure facility, BIF, Jamia Hamdard, Delhi, India

Running title: Synthesis and anti-inflammatory activity evaluation of 1,2,4-triazole derivatives

*To whom correspondence should be addressed: Sonu Chand Thakur, Ph.D., Centre for Interdisciplinary Research in Basic Sciences, Jamia Millia Islamia (Central University), Jamia Nagar, New Delhi 110025, India. Tel. /Fax: +91- 011-26981717; E-mail: sonuchandthakur@gmail.com, sthakur@jmi.ac.in

Authors contributed equally

Abstract

Substituted 1,2,4-triazole nucleus is common in several drugs used in a variety of clinical conditions including infections, hypoglycemia, hypertension and cancer. In this study, we synthesized 1,2,4-triazole and its 16 hydrazone derivatives (B1-B16), characterized them by IR, NMR and Mass spectroscopy, and evaluated their radical scavenging and anti-inflammatory activities *in vitro* and *in vivo*. Out of 16 derivatives, five (B1, B5, B6, B9, and B13) demonstrated a significant radical scavenging and anti-inflammatory activity *in vitro*. B6, which possessed two electron-donating hydroxyl groups, was most active among all. Molecular docking and MD simulation of the complex of B6 with prostaglandin-endoperoxide synthase (PTGS) or cyclooxygenase (COX) showed that B6 occupied celecoxib binding site in COX with high affinity (the binding free energy of the complex with COX-1 was -10.5, and -11.2 kcal/mol with COX-2). Maximum anti-inflammatory activity was also shown by the B6 derivative *in vivo*, in the rat model of carrageenan-induced inflammation. B6, along with four other derivatives (B1, B5, B9 and B13) exhibited 80-90% free radical scavenging activity. The IC₅₀ values of these compounds were $\geq 40\mu\text{M}$. Griess nitrite and dichloro-dihydro-fluorescein-diacetate assays suggested a significant inhibition of nitric oxide and reactive oxygen species, especially by B6 and B9. Taken together, out of 16 derivatives, B6 is reported to have highest anti-inflammatory and antioxidant activity at a low dose level, which may be attributed to its two electron-donating hydroxyls. B6 is proposed to be an important scaffold for the synthesis of new drugs against PTGS for use in a myriad of inflammatory and infectious diseases.

Supplementary material includes physical properties and spectral analysis data of synthesized derivatives.

Keywords: 1,2,4-triazole; molecular docking; MD simulation; inflammation; cyclooxygenases

Abbreviations:

ACS: American Chemical Society; COX: Cyclooxygenase; DCFH-DA: Dichloro-dihydro-fluorescein diacetate; DMSO-d₆: Deuterated dimethyl sulfoxide; DPPH: 2,2-Diphenyl-1-picrylhydrazyl; FTIR: Fourier transform infrared spectroscopy; LPS: Lipopolysaccharide; MD simulation: Molecular dynamic simulation; MTT: 3-(4,5-dimethylthiazol-2-yl)-2,5-diphenyltetrazolium bromide; NO: Nitric oxide; NPT: constants, Number (N), Pressure (P), and Temperature (T); NSAIDs: Non-steroidal anti-inflammatory drugs; NVT: constants, Number (N), Volume (V), and Temperature (T); OD: Optical density; PTGS: Prostaglandin-endoperoxide synthase; RNS: Reactive nitrogen species; ROS: Reactive oxygen species; TLC: Thin layer chromatography; TMS: Tetramethyl silane.

Introduction

Triazoles are heterocyclic compounds consisting of a 5-membered ring along with two carbon and three nitrogen atoms, which, on the basis of the position of nitrogen atom in the ring, can be divided into three isomers: (i) 1,2,3- triazole (vicinal triazole); (ii) 1,2,4- triazole (asymmetrical; asym- triazole); (iii) 1,3,4-triazole (symmetrical; sym- triazole) (Timur et al., 2018). Asym- or 1,2,4-Triazole is an interesting isomer of triazole which displays a number of pharmacologically important properties including the antioxidant (Pokuri, Singla, Bhat, & Shenoy, 2014), anti-inflammatory (Paprocka et al., 2015), anticancer (El-Sherief et al., 2018; Shahzad et al., 2019), antiviral (Kucukguzel, Tatar, Kucukguzel, Rollas, & De Clercq, 2008), antifungal (Dheer, Singh, & Shankar, 2017; Jin et al., 2018), antitubercular (S. Zhang et al., 2017), antibacterial (Eswaran,

Adhikari, & Shetty, 2009; Y. L. Fan, 2018), antimicrobial (Eswaran et al., 2009; Fan, Shi, & Bao, 2018), antitrypanosome (Papadopoulou et al., 2012), antiproliferative (Li et al., 2017), antibiotic (Xiao et al., 2014), analgesic (Gajanan Khanage, Raju, Baban Mohite, & Bhanudas Pandhare, 2013), anticonvulsant (Kapron et al., 2019), antidepressant (Kane, Dudley, Sorensen, & Miller, 1988), CNS stimulant, sedative, antianxiety and antimigraine (Genc et al., 2016; Kandile, Mohamed, & Ismaeel, 2017) properties. The wide range of biological activities of 1,2,4-triazole and its occurrence in common drugs including the anti-cancer (letrozole and anastrozole), anti-viral (ribavirin), anti-fungal (fluconazole, voriconazole, and itraconazole), anti-migraine (rizatriptan) and anti-anxiety (alprazolam) drugs has generated considerable amount of interest in 1,2,4-triazole moiety as a biologically active nucleus with potential implications as a scaffold for the synthesis of newer drugs.

Recent studies have demonstrated the effect of 1,2,4-triazole on lipophilicity, polarity and hydrogen bonding capacity of the compound, which may enhance its biological activity and improve physicochemical properties (Basri, Taha, & Ahmad, 2017; Gao, Wang, Xiao, & Huang, 2019; Kapron et al., 2019). Another interesting aspect of the 1,2,4-triazole nucleus is that it can exert diverse weak non-covalent interactions (hydrogen bonds, hydrophobic interactions, van der Waals interactions, coordination, ion-dipole, cation- π , π - π stacking etc.), which improve the solubility and the ability of binding to biomolecular targets (H. Z. Zhang, Damu, Cai, & Zhou, 2014) (C. Gao et al., 2019; J. Zhang, Wang, Ba, & Xu, 2019). Modification of 1,2,4-triazole may, therefore, be a useful approach in developing new triazole-based compounds with improved medicinal properties, and at a low dose level, with least or no toxicity and improved bioactivity. In literature, the nitrogen-containing heterocyclic compounds have been found useful

due to their broad range and significantly improved properties. Schiff bases of 1,2,4-triazoles are important nitrogen-containing heterocyclic compounds with potential bioactivity (Jin et al., 2018) and a Schiff base hydrazone nucleus might be a good candidate for designing and synthesis of new 1,2,4-triazole derivatives with excellent biological activity in a facile and easy synthesis (Kandile et al., 2017). In this study, we have designed, synthesized, and evaluated the biological activity, particularly the anti-inflammatory and antioxidative properties of 1,2,4-triazole and its derivatives, synthesized and characterized in our laboratory. The molecular docking and molecular dynamics (MD) simulation, a computer simulation approach to analyze the physical movements of atoms and molecules (which are allowed to interact for a fixed period of time) to get a view of the dynamic "evolution" of a complex or system, were performed to rationalize the potential of the chosen synthesized derivatives and elucidate its mechanism of action *in silico*. Synthesized compounds showed an affinity to PTGS, prostaglandin-endoperoxide synthase, a family of isozymes, commonly known as cyclooxygenase (COX) (EC 1.14. 99.1), which plays an important role in inflammation, cancer, and development. 1,2,4-Triazole and its selected derivatives are suggested in this study to provide a scaffold for the synthesis of new drugs in inflammation and other diseases where inhibition of PTGS may constitute one of the mechanisms of pathogenesis.

Materials and Methods

Chemicals and instruments

ACS grade chemicals were used for the synthesis in this study. For biological activity evaluation, chemicals/reagents were purchased from Sigma Aldrich and other standard commercial sources. The melting point (°C, uncorrected), wherever required, was recorded on a

Scitech melting point apparatus using capillary tubes closed at one end. For TLC, a pre-coated aluminum sheet, silica gel 60 F₂₅₄ (Merck) was used in a solvent system comprised of chloroform/methanol and hexane/ethyl acetate, 9:1ml. Spots were visualized under a UV lamp. Precursors, triazole, and substituted hydrazones were purified by silica gel column chromatography (pore size 60Å, 200-400 mesh) and eluted with chloroform/methanol and hexane/ethyl acetate. The elutants were concentrated in a Heidolph Laborota 4000 rotary evaporator and re-crystallized using chloroform/methanol and hexane/ethyl acetate. FTIR spectra were recorded in ATR mode in a Bruker Tensor 37 spectrophotometer. ν_{\max} was expressed as cm^{-1} . Mass spectra (ESI-MS) were recorded on an AB-Sciex 2000 instrument. ¹H NMR and ¹³C NMR spectra were recorded on a Bruker AVANCE (300 MHz) spectrometer using DMSO-d₆ as solvent with TMS as an internal standard. Chemical shifts were measured in hertz (Hz) and ppm on a δ scale. Splitting patterns were designated as follows: s, singlet; d, doublet; t, triplet; and m, multiplet.

Synthesis of 1,2,4-triazole and its derivatives (B1-B16)

1-Formylthiosemicarbazide (a) and 2H-1,2,4-triazole-3-thiol (b) were synthesized as described by Hu et al (Hu et al., 2013) with slight modifications. Ethyl 2-[5-(2-ethoxy-2-oxo-ethyl)sulfanyl-1,2,4-triazol-1-yl]acetate (c) and 2-[5-(2-hydrazino-2-oxo-ethyl)sulfanyl-1,2,4-triazol-1-yl]acetohydrazide (d) were synthesized by the procedure described by Wani et al (Wani, Bhat, Azam, & Athar, 2013). 1,2,4-Triazole derivatives were synthesized as follows: briefly, 0.01 mol of compound (d) was refluxed with 0.01 mol of appropriate aldehyde/ ketone and glacial acetic acid (1ml) in ethanol for 6-24h. Progress of the reaction was monitored by TLC (hexane: ethyl acetate, 9:1) / (chloroform: methanol, 9:1). The separated product was filtered and

washed with diethyl ether. Solvent was evaporated under reduced pressure to obtain the derivative in good yield. The compound was crystallized from ethanol/methanol/chloroform and air-dried.

Free radical scavenging and antioxidant activity evaluation

As shown in **Workflow 1**, all synthesized derivatives (B1-B16) were first evaluated for antioxidant activity *in vitro*, followed by biological activity evaluation in cell culture and *in vivo* studies on selected compounds in rat model of inflammation. Finally, molecular docking and molecular dynamics (MD) simulation analyses of the docked complex was performed to rationalize the potential of selected derivative (B6) found to have the maximum anti-inflammatory effect *in vivo* and to elucidate its mechanism of action *in silico* against PTGS.

2,2-Diphenyl-1-picrylhydrazyl (DPPH) assay

DPPH assay was performed by the protocol described by Manzocco et al (Manzocco, Anese, & Nicoli, 1998). Briefly, each synthetic derivative (0-800 µg/ml) was mixed with a methanolic solution followed by the addition of 150µl DPPH (1.3mg/ml). Optical density (OD) of the resulting mixture was measured at 517nm and the percentage inhibition was calculated as follows:

$$\text{Percent inhibition} = \frac{\text{OD}_{(\text{Control})} - \text{OD}_{(\text{Sample})}}{\text{OD}_{(\text{Control})}} \quad \text{Equation [1]}$$

Total reduction capability (TRC) assay

TRC was measured by the method described by Oyaizu (Oyaizu, 1986). Briefly, 2.5 ml of a 1% (w/v) solution of potassium ferricyanide hexacyanoferrate, $K_3Fe(CN)_6$ was mixed with 1ml of the test compound in 2.5ml of 0.2 M phosphate buffer (pH 6.6). The mixture was incubated for 20 minutes at 50°C in an incubator followed by the addition of 2.5ml of 10% trichloroacetic acid, 2.5ml distilled water and 0.5ml ferric chloride (0.1%, w/v). The absorbance of the reaction mixture was measured at 700nm against blank.

Nitric oxide radical scavenging assay

Nitric oxide (NO) radical scavenging activity was measured by the method described by Temraz and El-Tantawy (Temraz & El-Tantawy, 2008). Briefly, the test compound (concentration range, 10-800 $\mu\text{g/ml}$) was mixed with 20 mM sodium nitroprusside (2 ml) and the mixture was incubated at room temperature for 15 minutes followed by the addition of 1ml Griess reagent (1% sulphanimide, w/v, in 2% orthophosphoric acid, v/v, and 0.1% naphthyl ethylene diaminedihydrochloride, w/v). The mixture was vortexed and incubated in dark for 10 minutes and the development of pink color, an indication of the nitric oxide radical scavenging capability of the test compound, was measured at 540 nm against blank. Percent inhibition in activity was calculated as in Equation [1].

Cell culture studies

Murine blood macrophage cells, RAW 264.7 and J774.1A, purchased from the National Centre for Cell Science (NCCS), Pune were used to measure cell viability, nitrite and ROS. For all purposes, cells were maintained in 75 cm^2 culture flask containing DMEM supplemented with 10% FBS and 1% antibiotic solution in a humidified atmosphere at 5% CO_2 and 37 °C in a

water-jacketed CO₂ incubator (Thermo Fischer Scientific) (Routray & Ali, 2019). Cells were passaged 4-5 times.

Cytotoxicity

Test compounds were evaluated for their effect on cell viability or cytotoxicity as per the published protocols (Teng et al., 2012) . Briefly, cells (1×10^5) plated in a 96-well plate and treated with the test compound (5-160 μ M) were incubated in a CO₂ incubator at 37 °C (5% CO₂) for 48 h. After the incubation, the medium was discarded and an equal volume of serum free medium and MTT (20 μ L) was added into each well and the plate was further incubated at 37 °C for 3 h. Thereafter, 150 μ L DMSO was added to dissolve the formed formazan crystals. The plate was wrapped in foil and shaken on an orbital shaker for 15 minutes before taking the absorbance of the solution in a microplate reader at 570nm. The analysis was performed in triplicate (n=3). Data were expressed as Mean \pm SD. IC₅₀ was determined by the concentration-cell viability curve. The cell viability was calculated as follows:

$$\text{Cell viability} = (\text{Absorbance of the sample} / \text{Absorbance of control}) \times 100 \quad \text{Equation [2]}$$

Griess Nitrite assay

Nitrite in the culture medium was measured by the Griess colorimetric method (Routray & Ali, 2019). Briefly, cells (1×10^5 cells/ml) were plated in a 96-well plate and treated with the test compounds (B1, B5, B6, B9, and B13) and indomethacin as standard drug at a dose level of 40 μ M, IC₅₀. Cells were stimulated with the LPS (*Escherichia coli* O111:B4, 1g/mL) followed by

48h incubation at 37°C in a CO₂ incubator. The medium containing the cells (100µl) was mixed with an equimolar amount of Griess reagent and the absorbance of the reaction mixture was taken at 540nm in a microplate reader using a sodium nitrite solution to draw the standard calibration curve. For statistical analysis, one-way ANOVA was used followed by Dunnett's multiple comparison tests.

Dichloro-dihydro-fluorescein diacetate (DCFH-DA) assay

Production of ROS by the LPS-stimulated macrophage was analyzed by the DCFH-DA assay (Pan et al., 2014). Briefly, cells were treated with 40, 80 or 160µM of the test compound in culture medium incubated at 37°C in a CO₂ incubator for 48 h, followed by the stimulation with LPS for 30 minutes. DCFH-DA (10µM) was used to detect the ROS level as per the published procedure and the fluorescence was measured in a Jasco spectrofluorometer (FP-6200) after excitation at 485 nm, and an emission wavelength of 500-550nm, respectively.

Computational analysis: molecular docking and MD simulation

The binding modes of selected synthetic derivatives (B1, B5, B6, B9 and B13) with PTGS (COX) were understood by the molecular docking and MD simulation analysis of each complex. Chemical structures of COX-1 (PDB ID: 3KK6) and COX-2 (PDB ID: 5KIR) were obtained from the protein databank, PDB (www.rcsb.org/pdb) and converted to three-dimensional structures (3D) in ChemBio3D Ultra 12.0 and saved (Shinkafi et al., 2019). Docking simulations were studied by the Lamarckian genetic algorithm method (Morris et al., 1998). Standard docking procedure was employed for rigid protein and flexible ligand, whose torsion angles were identified for 10 independent runs per ligand. Docking grids were generated through bound co-

crystallized ligand. A grid of 28, 28, and 32 points in x, y, and z directions was built with a grid spacing of 0.375 Å. Distance-dependent function of the dielectric constant was used for calculating the energy maps. Default settings were used for other parameters. Docking parameters were validated by re-docking of co-crystal ligand at the catalytically active site of COX. At the end of the docking procedure, analysis of best pose interaction was done through The PyMOL Molecular Graphics System, Maestro10.5 visualizer, and Chimera 1.11.

Two independent sets of MD simulations were run to understand the binding affinities and binding modes of the compounds of interest – one set was performed with COX-1 (without celecoxib and co-crystal celecoxib) and the docked complex system (celecoxib docked and compound B6 docked), while another set was performed for COX-2 and docked complex system (celecoxib docked and B6 docked) using Gromacs v5.1.2. The X-ray crystal structure of COX-1 and COX-2 was recruited from PDB. Before performing the simulation, the wild type of each target was solvated in an octahedral TIP3P water box and relaxed at neutral pH for 500 ps. The last frame of the trajectory obtained after the relaxation of wild type targets in water, was used. Through steepest descent method, the entire system was minimized for 10,000 steps, followed by minimization of another 10,000 steps by conjugate gradient method at 10 K to 277.15 K, through Langevin thermostat in canonical (NVT) ensemble (Pastor, Brooks, & Szabo, 1988; Uberuaga, Anghel, & Voter, 2004). Then, 100 ps simulation was performed under constant temperature and pressure under the isothermal-isobaric (NPT) ensemble. The whole protein and solvent system was minimized for 5,000 steps and heated from 10 K to 300 K for 100 ps in the NVT ensemble. The production run for each protein was carried throughout 40 ns through the NPT ensemble. All simulations conducted in this study involved a time step of 2 fs. Root mean square deviation

(RMSD), angles, and root mean square fluctuation (RMSF) were determined through Gromacs in built tools, *g_rms*, *g_sgangle*, and *g_rmsf*, respectively.

Animal studies

Animals. The anti-inflammatory activity of selected test compounds was demonstrated in rat against carrageenan-induced paw edema. Briefly, adult Wistar strain of rat, weighing 120-180 g, was used for the study. Animals were acclimatized for one week before starting the experiment. All animals were kept in an environmentally controlled room maintained at 30-70% relative humidity, 18-26 °C room temperature and a 12 h light/ dark cycle, and at least 10 room air changes per hour. Animals were housed in polypropylene rat cages in a group containing not more than six rats (n=6). Animals had free access to laboratory chow and water *ad libitum*. The study was approved by the Institutional Animal Ethics Committee, and all experiments were performed as per the guidelines laid down by the CPCSEA, the Committee for the Purpose of Control and Supervision of Experiments on Animals (Registration No. 173-CPCSEA).

Treatment protocol and dose levels. Rats were randomly divided into 7 different groups (6 rats in each group). Inflammation was induced in hind paw of each rat by injecting a suspension of 0.1 ml of 1% carrageenan in normal saline in the sub planter region as described by Winter et al., 1962 (Winter, Risley, & Nuss, 1962). The test compound, suspended in tween 80 (1%, w/v), was administered orally 1 h prior to the injection of carrageenan at a dose level of 5, 10, or 20 mg/kg body weight orally. Indomethacin was used as standard drug at a dose level of 5 mg/kg body weight by the same route. Normal control group of animals did not receive any treatment. The group of animals injected with carrageenan alone served as negative control to study the

suppression of inflammation by the drug. The paw volume was measured at 1, 3 and 5h post-carrageenan injection with a Vernier caliper. Change in paw volume or percent inhibition by the test drug was calculated as follows: Percent inhibition = $(V_c - V_t) / V_c \times 100$, where V_c is mean increase in paw volume by the carrageenan injection and V_t , the mean increase in paw volume in treatment group. Potency of the test compound relative to indomethacin was calculated as follows: Potency = Percent inhibition obtained after the treatment with test compound / Percent inhibition after treatment with standard drug.

Statistical analysis

Graph Pad Prism version 6.0 was used for all statistical analysis. Each value represents Mean \pm SD of analysis in triplicate, or n=6, for studies on animals. Statistical difference between standard and test compounds was determined using a two-tailed Student's *t*-test. Differences were considered significant at $p \leq 0.05$ (* $p < 0.05$, ** $p < 0.01$, *** $p < 0.001$, **** $p < 0.0001$).

Results

Synthesis and structural determination

1,2,4-Triazole and its 16 derivatives were synthesized as per the newly designed synthetic route outlined in **Scheme1**, using thiosemicarbazide (Sigma Aldrich) as starting material without further purification.

The reaction of thiosemicarbazide with formic acid resulted in the synthesis of 1-formylthiosemicarbazide, the intermediate which reacts with 10% KOH and form 2H-1,2,4-triazole-3-thiol (due to the removal of water molecule). Esterification of 2H-1,2,4-triazole-3-thiol with ethylchloroacetate forms ethyl 2-[5-(2-ethoxy-2-oxo-ethyl)sulfanyl-1,2,4-triazol-1-yl]acetate which when reacted with hydrazine hydrate forms 2-[5-(2-hydrazino-2-oxo-ethyl)sulfanyl-1,2,4-triazol-1yl]acetohydrazide. Finally, the reaction of hydrazide with different aldehydes and ketones yielded different derivatives (B1-B16). Various substituted R groups are depicted in **Table 1**. The yield was good and the compounds could be easily recrystallized using chloroform and methanol.

The structures of all newly synthesized compounds were confirmed by the FTIR, ^1H NMR, ^{13}C NMR, and ESI-MS. The physical properties and the results of the spectral analysis data of all derivatives are shown in supplementary files, **Supplementary material, S1 and S2**, respectively. The presence of sharp bands in IR spectra around $650\text{-}750\text{ cm}^{-1}$ and $1040\text{-}1095\text{ cm}^{-1}$ signify the peaks corresponding to C-S and C-N. Simultaneously appearance of the peaks of C=O, C=N and NH in $1600\text{-}1675\text{ cm}^{-1}$, $3100\text{-}3200\text{ cm}^{-1}$ supports the synthesis of different derivatives, B1-B16. In ^1H NMR spectra, the singlet for N=C-H of the triazole ring, S-CH₂ and N-CH₂ at 7.43-9.75, 3.27-3.98 and 4.05-5.03 ppm was achieved. Also, the singlet for -NH of hydrazone was achieved from 8.60-11.99 ppm, followed by multiplets of aromatic protons at 6.71-8.16 ppm for B1-B16. The carbon NMR also confirmed the formation of the desired derivatives, B1-B16, with signals at 40.33-53.22 ppm for CH₂, carbon bonded to -S and -N atoms. The clear signal at 153.52-173.54 ppm appeared for the C=O group of the synthesized hydrazone. Singlet indicating the formation of the C=N bond appeared at 161.21-170.04 ppm.

The appearance of the desired characteristic peaks confirmed the formation of respective compounds. In the Mass spectra (ESI-MS), the appearance of the molecular ion peaks at desired intensities, corresponding to the molecular weight of the compounds (B1-B16), further confirmed the formation of derivatives.

Free radical scavenging activity and TRC

As per the flow chart **Workflow 1**, synthesized derivatives were first tested for efficacy *in vitro*. All 16 derivatives had considerable antioxidant activity, with maximum DPPH radical scavenging activity exhibited by B13 ($95.45 \pm 0.64\%$) and an almost similar activity by B6 ($95.31 \pm 0.12\%$), followed by B9 ($91.67 \pm 1.20\%$), B1 ($88.69 \pm 1.05\%$) and B5 ($80.98 \pm 3.40\%$), when compared with the positive control L-ascorbic acid (L-AA) ($95.36 \pm 1.24\%$) at $800\mu\text{g/ml}$ (**Fig. 1(A)(B)**). B1, B6, B9 and B13, which possess electron-donating ($-\text{OCH}_3$, $-\text{OH}$ and $-\text{CH}_3$) groups as a substituent, displayed better free radical scavenging activity than B5 (which has an electron-withdrawing nitro ($-\text{NO}_2$) group as a substituent). The radical scavenging activity of these compounds was comparable to the standard substance, L-AA. IC_{50} of B1, B5, B6, B9 and B13 were 82.88 ± 1.732 , 179.69 ± 1.05 , 38.79 ± 1.88 , 43.30 ± 1.79 , and $55.66 \pm 0.53 \mu\text{g/ml}$ ($p < 0.001$), respectively, when compared with L-AA ($35.58 \pm 1.52 \mu\text{g/ml}$) (**Table 2**). The total reduction capability among all compounds was best for B1, B5, B6, B9, and B13. B6 TRC, expressed as absorbance at 700 nm, increased from 0.176 ± 0.017 at $10\mu\text{g/ml}$ to 2.639 ± 0.170 at $800\mu\text{g/ml}$ (**Fig. 2**). TRC of B1, B5, B9 and B13 at $800\mu\text{g/ml}$ was in the following order: B9 (2.205) > B13 (1.924) > B1 (1.079) > B5 (0.697). In comparison, TRC of L-AA was 2.602 . B5 reported the lowest activity among all derivatives, while B6 showed the highest activity in a

concentration-dependent manner, reflecting the potential of B6 to reduce the transition state of iron.

Nitric oxide radical scavenging activity

Results of the nitric oxide radical scavenging activity of 1,2,4-triazole derivatives are shown in **Fig. 3(A)**. A remarkable inhibitory effect was observed with B1, B5, B6, B9 and B13 in a concentration-dependent manner in the following order: B6 ($92.55 \pm 1.18\%$), B9 ($88.65 \pm 2.22\%$), B13 ($88.03 \pm 1.94\%$), B5 ($83.49 \pm 1.72\%$) and B1 ($79.75 \pm 2.46\%$), when compared with L-AA ($94.31 \pm 0.99\%$) at $800\mu\text{g/ml}$, as shown in **Fig. 3(B)**. IC_{50} values for B1, B5, B6, B9 and B13 were in the following order, 57.29 ± 1.73 , 60.49 ± 1.72 , 32.40 ± 0.62 , 36.33 ± 1.71 , $37.39 \pm 1.94 \mu\text{g/ml}$ ($p < 0.001$), respectively. IC_{50} of the standard was $43.46 \pm 1.3 \mu\text{g/ml}$ (**Table 2**).

Synthesis and secretion of free radicals by the stimulated macrophages and cell viability

As shown in **Fig. 4(A)(B)**, IC_{50} of B1, B5, B6, B9 and B13 was $\geq 40\mu\text{M}$ (**Table 3**). There was a significant reduction (70-80%) in NO production by the LPS-stimulated macrophages by B1, B5, B6, B9 and B13 in comparison to indomethacin, as shown in **Fig. 5(A)(B)** and **Table 4**. The extent of inhibition was more in case of B6 and B9. The intracellular antioxidant activity, as measured by the DCFH-DA assay, was also high particularly in the presence of B6 and B9, as reported in **Fig. 6(A)(B)** and **Fig. 7(A)(B)**, at 40, 80 and $160\mu\text{M}$.

In vivo anti-inflammatory activity

B1, B6, B9 and B13, which showed good radical scavenging activity *in vitro*, demonstrated a good anti-inflammatory activity *in vivo* at a dose level of 5, 10, and 20 mg/kg body weight when administered orally in rats (**Fig. 8, Table 5**). B6 exhibited the most significant anti-inflammatory activity (64.44% inhibition and a potency of 0.92 at 20mg/kg body weight after 5h of inducing inflammation). The effect was comparable to the standard drug indomethacin (potency, 1.00) (**Table 5**). The percentage inhibition of edema for B1, B9 and B13 was 58.4, 61.21 and 62.27%, respectively, after 5 h. The order of the anti-inflammatory activity demonstrated by B1, B6, B9 and B13 was as follows: B6 > B13 > B9 > B1.

Molecular docking and MD simulation

Molecular docking studies were carried out to rationalize the potential of chosen synthesized compounds as anti-inflammatory agents by predicting their binding affinities, binding mode, and proper orientation with PTGS or COX against co-crystal ligand celecoxib. The compounds B1, B5, B6, B9, and B13, which exhibited good anti-inflammatory activity, were docked in the catalytic binding pocket of COX-1 (PDB ID: 3KK6) and COX-2 receptor (PDB ID: 5KIR) with reference to celecoxib as a co-crystal ligand. The binding free energies of these five derivatives complexed with COX-1 and COX-2 are shown in **Table 6**.

The binding of celecoxib with catalytic ligand-binding pocket of COX-1 is considered to be a complex interaction *via* Gln 192, Leu 352, Phe 518 and Ile 517 hydrogen bonding network resulting in tight binding. Celecoxib also formed important hydrophobic interaction with Val 116, Val 349, Tyr 355, Ile 359, Leu 384, Trp 387, Met 522, Ile 523, Ala 527 and Leu 531 (**Table 6, Fig. 9(C)(D)**). B6 was found to bind into the same ligand-binding pocket of COX-1 as

celecoxib (interaction energy, 10.5kcal/mol). Three H-bonding interactions between *para*-hydroxyl of B6 with Arg 120, Leu 352, and Phe 518 of COX-1 active sites were observed (**Fig. 9(A)(B)**). B6 also exhibited the hydrophobic interaction with Phe 205, Phe 209, Val 228, Val 344, Tyr 348, Val 349, Tyr 355, Leu 359, Ile 377, Phe 381, Tyr 385, Trp 387, Ile 517, Met 522, Ile 523, Ala527, Leu 531 and Leu 534 (**Fig. 9(B)**). It superimposed with the co-crystal ligand celecoxib which displayed the same interaction in the catalytic domain of COX-1. The aromatic moiety attached to the triazole ring of B6 was superimposed on the aromatic moiety with the sulfonamide functional group of celecoxib (**Fig.11(A)**). B6 (*para*-hydroxyl substituted) showed similar docking results as celecoxib and exhibited excellent docking with COX-1. B1, B5, B6, B9 and B13 also docked in the active site of COX-2 (PDB ID: 5KIR). Celecoxib binds through a network of hydrogen bonding with Gln 192, Leu 352, Ser 353, Arg 513 and Phe 518, and (also) forms hydrophobic interaction with Val 116, Val 349, Tyr 355, Ile 359, Leu 384, Trp 387, Ala 516, Ile 517, Met 522, Val 523, Ala 527 and Leu 531(**Fig. 10(C)(D)**). B6 exhibited similar interactions in the catalytic ligand binding site of COX-2. The interaction energy was 11.2kcal/mol. B6 showed four hydrogen bonding interactions between *para*-hydroxyl (of B6) with Gln 192, Leu 352, Asn 375, and Ile 517 in COX-2 active site. It had hydrophobic interaction with Phe 205, Phe 209, Val 228, Val 344, Tyr 348, Val 349, Tyr 355, Ile 377, Phe 381, Tyr 385, Trp 387, Ala 516, Phe 518, Met 522, Ile 523, Ala 527, Phe 529, and Leu 534(**Fig. 10(A)(B)**). In order to see the positioning of B6 in the catalytic domain of COX-2, superimpositions were performed with the co-crystal ligand celecoxib which displayed almost similar interaction in the catalytic domain of COX-2 (**Fig. 11(B)**). To sum up, results of the *in-silico* analyse suggested anti-inflammatory activity via PTGS.

For a better understanding of the binding affinity and binding mode, the complex docked with the compound showing highest docking score, B6, was subjected to MD simulation for 40 ns in an aqueous environment at 300K. An analysis of RMSD, RMSF, Rg and SASA suggested structural stability of the ligand (B6)-PTGS complex. The examination of all C- α and backbone RMSD suggested conformational stability of COX-1 and COX-2 in an aqueous environment. The trajectory obtained for COX-1 (3KK6_Without celecoxib (black)) achieved equilibrium after 19 ns (**Fig. 12(A)(B)**) and a stable conformation of COX-1 can be seen up to 36 ns with minor fluctuation. Thereafter, the trajectory showed a sharp transition for a few nanoseconds and dropped to attain equilibrium at 40 ns. The trajectory obtained for protein-celecoxib co-crystal structure (blue) showed equilibrium achieved at 9 ns followed by fluctuation of RMSD in an average of 0.3 nm toward 22 ns. A further increase of RMSD started after 22 ns and reached up to 2.7 nm at 35 ns, followed by a short decrease (toward 2.2 nm) at 40 ns with small fluctuations. RMSD of docked celecoxib (red) showed a sharp increase up to 2.2 nm at 13 ns followed by the equilibrium of the structure up to 40 ns with an average fluctuation of 0.8 nm. On the other hand, B6 docked COX-1 (green) showed a slow increase at 6 ns, and the structure maintained an equilibrium toward 40 ns with an average fluctuation of 0.5 nm. The change in RMSD with respect to COX-1 without celecoxib suggest a tight binding (of celecoxib, as well as B6) in the active region. The ligand was stabilized by hydrogen and hydrophobic interactions with surrounding residues during the simulation period. B6 stabilized the complex more quickly than celecoxib. COX-2 (black) showed a sharp increase in RMSD in first 12.5 ns, followed by equilibrium at ~25.5 ns. Thereafter, trajectory showed a small increase up to 32.5 ns followed by a small increase up to 39 ns; afterward, trajectory attained equilibrium at 40 ns. Celecoxib docked structure of 5KIR (red) and B6 docked 5KIR (green) achieved equilibrium after 11 ns

and thereafter, the complexes fluctuated with an average RMSD of 0.6 nm and 0.7 nm throughout the simulation run. In short, data suggest large conformational changes when celecoxib or B6 bound to COX-2 (**Fig. 13(A)(B)**). The variation in conformation due to ligand contributes to the stabilization of COX-2 upon binding.

The Radius of gyration (Rg), which is the weighted root mean square average of the distance of all scattering atoms from the center of mass of the protein and which provides information of the overall structural compactness of protein, is important to understand the conformational changes and dynamic stability of the complexes in an aqueous environment. As shown in **Fig.12(C)(D)**, the secondary and tertiary structures of COX-1 (and its complexes with the ligand) remained stable during the simulation run (40ns). Average Rg for the B6 complex remained low (~2.3 nm), whereas docked celecoxib complex showed a slight increase to 2.325nm. A comparative analysis of the results suggested very less increase in compactness of the protein structures both in co-crystal and B6 complexes, as compared with native COX-1 (removed celecoxib from co-crystal). Rg analysis (COX-2 and COX-2–ligand complex) (**Fig. 13(C)(D)**) showed a change in Rg of the docked complex (COX-2-B6) from 2.4 nm to 2.325 nm at 3 ns, followed by equilibrium up to 40 ns with only minor fluctuation. In case of COX-2-celecoxib, Rg started from 2.4 nm and reached to 2.315 nm at 5 ns. After that, the complex maintained equilibrium up to 25 ns and thereafter, a sudden decrease was observed up to 2.26 nm at 27 ns followed by equilibrium toward 40 ns with small fluctuations. The residual fluctuation in docking complexes was around 0.1-0.3 nm and was lower than the native (removed celecoxib from co-crystal)(**Fig. 12(E)**). Moreover, the active site protein residues interacting with docked ligands showed a little fluctuation and stabilized in their favorable conformations. RMSF values further illustrated that

N-terminal part of COX-1 native and complex showed more fluctuations than C-terminal part. A comparative analysis of COX-2 and COX-2-B6 complex demonstrated fluctuations in 0.1-0.3 nm range at the catalytic site of COX-2 (**Fig. 13(E)**). On the other hand, little fluctuation was detected at the same catalytic site of COX-2 with celecoxib, as well as COX-2-B6 complex. Apart from this, we observed a high level of mobility in some parts of COX-2, as well as COX-2-ligand complexes, but these were not considered as our focus was to study the dynamic behavior at the catalytic site. SASA, the solvent-accessible surface area, of COX-1 and the docked complex (**Fig. 12(F)**) showed an average area of 309 nm² and 311 nm² with the native removed celecoxib from co-crystal and native protein-celecoxib co-crystal structure of COX-1. Docked complexes COX-1-celecoxib and COX-1-B6 were exposed to solvent environment with an average area of 314 and 310 nm². It can be concluded that the docked complex (B6) showed either similar SASA or lower to native (without celecoxib). The lower value of SASA obtained from the complex suggested that B6 on binding to COX-1 active site may lead to a tight packing of hydrophobic residues aligned at the core of the active site. SASA of COX-2 and docked complex (**Fig. 13(F)**) showed an average area of 327 nm²; the docked complexes (COX-2-celecoxib and COX-2-B6) had an average area of 308 nm² and 305 nm², respectively. A lower SASA for COX-2-celecoxib and COX-2-B6, when compared to COX-2, clearly suggested that these compounds, when interacted with COX-2 active site, may lead to a tight packing of hydrophobic residues aligned at the core of the active site.

Discussion

The heterocyclic compounds are commonly used in designing and development of newer classes of medicinally important structural moieties with improved biological and pharmacological properties such as the antimicrobial (Eswaran et al., 2009; Fan et al., 2018),

antibacterial (Eswaran et al., 2009; Y. L. Fan, 2018), anti-inflammatory (Paprocka et al., 2015), analgesic (Gajanan Khanage et al., 2013), anticonvulsant (Kapron et al., 2019), and anticancer properties (El-Sherief et al., 2018; Shahzad et al., 2019), to name a few. Triazole is an important heterocyclic moiety possessing a five-membered ring along with two carbon and three nitrogen atoms. Triazole and its derivatives are known for their diverse and a wide range of biological activities. Many studies have shown that the biological activities of 1,2,4-triazole and its derivatives are due to the existence of the 1,2,4-triazole nucleus (Q. Zhang et al., 2007). Some of the compounds with triazole ring are reported as potent anticancer CA-4 analogues (Mur Blanch et al., 2012). The presence of S-linkers in the structure improves some drug-like parameters such as increasing water solubility, decreasing lipophilicity, and offering good hydrogen bond acceptors (Bogolubsky et al., 2015). 1,2,4-Triazole along with Schiff base hydrazone ligands are known to display excellent pharmacological activities, including the ability to inhibit oxidative stress (Pokuri et al., 2014) and inflammation (Paprocka et al., 2015), which have been reported to play an important role in the pathogenesis of many diseases, ranging from infection to cancer. In this study, we have synthesized a new series of hydrazone derivatives of 1,2,4-triazole (**Scheme 1**). All synthesized derivatives were obtained in good yield and had sharp melting points. The newly synthesized moieties were characterized by FTIR, ^1H NMR, ^{13}C NMR, and ESI-MS. From proton (^1H) NMR spectra, the singlet for N=C-H of the triazole ring, S-CH₂, and N-CH₂ at 7.43-9.75 ppm, 3.27-3.98 ppm and 4.05-5.03 ppm was achieved. Also, the singlet for -NH of hydrazone was achieved from 8.60-11.99 ppm, followed by multiplets of aromatic protons at 6.71-8.16 ppm for B1-B16. The appearance of desired peaks at respective intensities confirmed the formation of derivatives. All 16 derivatives (B1-B16) when evaluated *in vitro* for antioxidant and anti-inflammatory activity by the DPPH assay, TRC and NO assays showed significant

activities when compared with known antioxidant and anti-inflammatory substance, L-ascorbic acid. B6, which has electron-donating-OH as ring substituent easily stabilized the DPPH free radical, displaying antioxidant activity, and enhanced the reductive ability by conversion of ferricyanide complex Fe^{3+} to ferrous form. B6 also showed a significant nitric oxide radical scavenging activity with an IC_{50} of $32.40 \pm 0.62 \mu\text{g/ml}$. Excessive and rapid production of both reactive oxygen and reactive nitrogen species occurs during various inflammation-related diseases and its mitigation has been found to be beneficial in a number of pathological conditions (Afonso, Champy, Mitrovic, Collin, & Lomri, 2007). We also studied the cytotoxicity of B6 and found it to be much less cytotoxic in MTT assay in RAW 264.7 and J774.1A cells. The compound significantly suppressed the nitric oxide radical production by the LPS-primed macrophages. The effect was comparable to indomethacin, a standard drug used in this study. The level of ROS is also reported to be significantly reduced in this study by B6. *In vivo* evaluation of the activity of B6 in rat model of carrageenan-induced inflammation (rat paw edema inhibition by the drug) confirmed the anti-inflammatory action of the drug. B6 caused a significant reduction in the size of edema.

In order to rationalize the potential of B6 as a novel synthetic drug with appreciable anti-inflammatory activity, binding mode of the selected derivative, B6, and its proper orientation in the active site of a key enzyme involved in inflammation, PTGS or COX was studied, against co-crystal ligand celecoxib. The docking analysis suggested that the most active derivative identified in this study, B6, nicely binds to COX-1 ($\Delta G_{(\text{Binding})} = -10.5 \text{ kcal/mol}$) and COX-2 ($\Delta G_{(\text{Binding})} = -11.2 \text{ kcal/mol}$). MD simulation of B6 and the standard revealed stability of the complex with both COX-1 and COX-2. The interaction was consistent with the essential active

site residues during the period of simulation. The activity of B6 may be attributed to the presence of phenyl ring with two hydroxyl groups as substituents. This study implicates B6 as an important scaffold for the synthesis of new medicinal agents in inflammatory conditions. A graphical representation depicting the beneficial effects of B6 is shown in **Fig. 14**.

Conclusions

This study reports the synthesis, characterization and free radical scavenging and anti-inflammatory activity of 1,2,4-triazole and its hydrazone derivatives. The structure of the synthesized compounds was confirmed by IR, ¹H NMR, ¹³C NMR and MS. Out of 16 derivatives, five (B1, B5, B6, B9, B13) (IC₅₀≥40 μM) demonstrated 80-90% free radical scavenging and antioxidant activity at low dose level; in particular, B6 and B9 significantly ameliorated the reactive oxygen species and nitrite production by the LPS-stimulated macrophages in culture. B6 demonstrated a significant anti-inflammatory effect in animal model of inflammation. Computational studies suggested stability of the B6-PTGS / COX complex, and its binding free energies, against bound co-crystal ligand celecoxib—the interaction was similar to celecoxib, and the resulting complex was strong and stable. The presence of phenyl ring with two hydroxyl groups as substituents in B6 is suggested to explain a better B6 efficacy, implicating B6 as an important scaffold for the synthesis of new compounds targeted against PTGS in inflammation and infections.

Acknowledgements

BK acknowledges UGC for Maulana Azad National Fellowship. BK expresses her gratitude to Professor Faizan Ahmad, for his unconditional support, advice and guidance. AN acknowledges

the Indian Council of Medical Research (ICMR) for Senior Research Fellowship. SA acknowledges the DBT Bioinformatics infrastructure facility, BIF, Jamia Hamdard under BTISNet.

Conflict of Interest

The authors declare no conflict of interest.

References

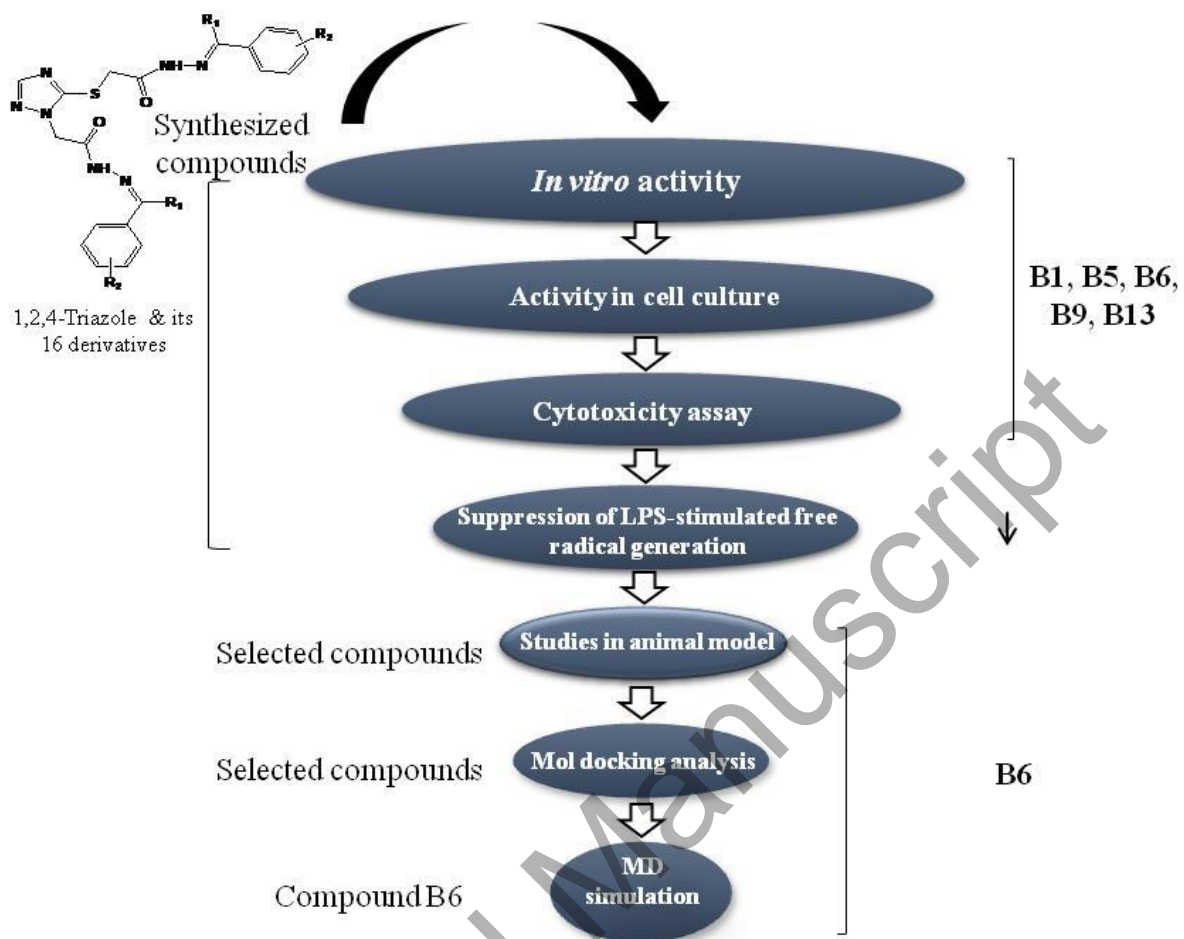
- Afonso, V., Champy, R., Mitrovic, D., Collin, P., & Lomri, A. (2007). Reactive oxygen species and superoxide dismutases: role in joint diseases. *Joint Bone Spine*, *74*(4), 324-329. doi: S1297-319X(07)00159-5 [pii] 10.1016/j.jbspin.2007.02.002
- Basri, A. M., Taha, H., & Ahmad, N. (2017). A Review on the Pharmacological Activities and Phytochemicals of *Alpinia officinarum* (Galangal) Extracts Derived from Bioassay-Guided Fractionation and Isolation. *Pharmacogn Rev*, *11*(21), 43-56. doi: 10.4103/phrev.phrev_55_16 PRev-11-43 [pii]
- Bogolubsky, A. V., Moroz, Y. S., Mykhailiuk, P. K., Ostapchuk, E. N., Rudnichenko, A. V., Dmytriv, Y. V., . . . Tolmachev, A. (2015). One-Pot Parallel Synthesis of Alkyl Sulfides, Sulfoxides, and Sulfones. *ACS Comb Sci*, *17*(6), 348-354. doi: 10.1021/acscombsci.5b00024
- Dheer, D., Singh, V., & Shankar, R. (2017). Medicinal attributes of 1,2,3-triazoles: Current developments. *Bioorg Chem*, *71*, 30-54. doi: S0045-2068(16)30332-7 [pii] 10.1016/j.bioorg.2017.01.010
- El-Sherief, H. A. M., Youssif, B. G. M., Abbas Bukhari, S. N., Abdelazeem, A. H., Abdel-Aziz, M., & Abdel-Rahman, H. M. (2018). Synthesis, anticancer activity and molecular modeling studies of 1,2,4-triazole derivatives as EGFR inhibitors. *Eur J Med Chem*, *156*, 774-789. doi: S0223-5234(18)30580-4 [pii] 10.1016/j.ejmech.2018.07.024
- Eswaran, S., Adhikari, A. V., & Shetty, N. S. (2009). Synthesis and antimicrobial activities of novel quinoline derivatives carrying 1,2,4-triazole moiety. *Eur J Med Chem*, *44*(11), 4637-4647. doi: 10.1016/j.ejmech.2009.06.031 S0223-5234(09)00360-2 [pii]
- Fan, Z., Shi, J., & Bao, X. (2018). Synthesis and antimicrobial evaluation of novel 1,2,4-triazole thioether derivatives bearing a quinazoline moiety. *Mol Divers*, *22*(3), 657-667. doi: 10.1007/s11030-018-9821-8 10.1007/s11030-018-9821-8 [pii]
- Gajanan Khanage, S., Raju, A., Baban Mohite, P., & Bhanudas Pandhare, R. (2013). Analgesic activity of some 1,2,4-triazole heterocycles clubbed with pyrazole, tetrazole, isoxazole and pyrimidine. *Adv Pharm Bull*, *3*(1), 13-18. doi: 10.5681/apb.2013.003
- Gao, C., Chang, L., Xu, Z., Yan, X. F., Ding, C., Zhao, F., . . . Feng, L. S. (2019). Recent advances of tetrazole derivatives as potential anti-tubercular and anti-malarial agents. *Eur*

- J Med Chem*, 163, 404-412. doi: S0223-5234(18)31038-9 [pii] 10.1016/j.ejmech.2018.12.001
- Gao, F., Wang, T., Xiao, J., & Huang, G. (2019). Antibacterial activity study of 1,2,4-triazole derivatives. *Eur J Med Chem*, 173, 274-281. doi: S0223-5234(19)30358-7 [pii] 10.1016/j.ejmech.2019.04.043
- Genc, M., Karagoz Genc, Z., Tekin, S., Sandal, S., Sirajuddin, M., Hadda Taibi, B., & Sekerci, M. (2016). Design, Synthesis, in vitro Antiproliferative Activity, Binding Modeling of 1,2,4,-Triazoles as New Anti-Breast Cancer Agents. *Acta Chim Slov*, 63(4), 726-737. doi: Genc-2014-4 [pii] 10.17344/acsi.2016.2428
- Hu, J., Wang, Y., Wei, X., Wu, X., Chen, G., Cao, G., . . . Li, X. (2013). Synthesis and biological evaluation of novel thiazolidinone derivatives as potential anti-inflammatory agents. *Eur J Med Chem*, 64, 292-301. doi: 10.1016/j.ejmech.2013.04.010 S0223-5234(13)00242-0 [pii]
- Jin, R. Y., Zeng, C. Y., Liang, X. H., Sun, X. H., Liu, Y. F., Wang, Y. Y., & Zhou, S. (2018). Design, synthesis, biological activities and DFT calculation of novel 1,2,4-triazole Schiff base derivatives. *Bioorg Chem*, 80, 253-260. doi: S0045-2068(18)30272-4 [pii] 10.1016/j.bioorg.2018.06.030
- Kandile, N. G., Mohamed, M. I., & Ismaeel, H. M. (2017). Synthesis of new Schiff bases bearing 1,2,4-triazole, thiazolidine and chloroazetidine moieties and their pharmacological evaluation. *J Enzyme Inhib Med Chem*, 32(1), 119-129. doi: 10.1080/14756366.2016.1238365
- Kane, J. M., Dudley, M. W., Sorensen, S. M., & Miller, F. P. (1988). 2,4-Dihydro-3H-1,2,4-triazole-3-thiones as potential antidepressant agents. *J Med Chem*, 31(6), 1253-1258. doi: 10.1021/jm00401a031
- Kapron, B., Luszczki, J. J., Plazinska, A., Siwek, A., Karcz, T., Grybos, A., . . . Plech, T. (2019). Development of the 1,2,4-triazole-based anticonvulsant drug candidates acting on the voltage-gated sodium channels. Insights from in-vivo, in-vitro, and in-silico studies. *Eur J Pharm Sci*, 129, 42-57. doi: S0928-0987(18)30553-0 [pii] 10.1016/j.ejps.2018.12.018
- Kucukguzel, I., Tatar, E., Kucukguzel, S. G., Rollas, S., & De Clercq, E. (2008). Synthesis of some novel thiourea derivatives obtained from 5-[(4-aminophenoxy)methyl]-4-alkyl/aryl-2,4-dihydro-3H-1,2,4-triazole-3-thiones and evaluation as antiviral/anti-HIV and anti-tuberculosis agents. *Eur J Med Chem*, 43(2), 381-392. doi: S0223-5234(07)00192-4 [pii] 10.1016/j.ejmech.2007.04.010
- Li, Y. H., Zhang, B., Yang, H. K., Li, Q., Diao, P. C., You, W. W., & Zhao, P. L. (2017). Design, synthesis, and biological evaluation of novel alkylsulfanyl-1,2,4-triazoles as cis-restricted combretastatin A-4 analogues. *Eur J Med Chem*, 125, 1098-1106. doi: S0223-5234(16)30913-8 [pii] 10.1016/j.ejmech.2016.10.051
- Manzocco, L., Anese, M., & Nicoli, M. C. (1998). Antioxidant Properties of Tea Extracts as Affected by Processing. *LWT - Food Science and Technology*, 31(7-8), 694-698

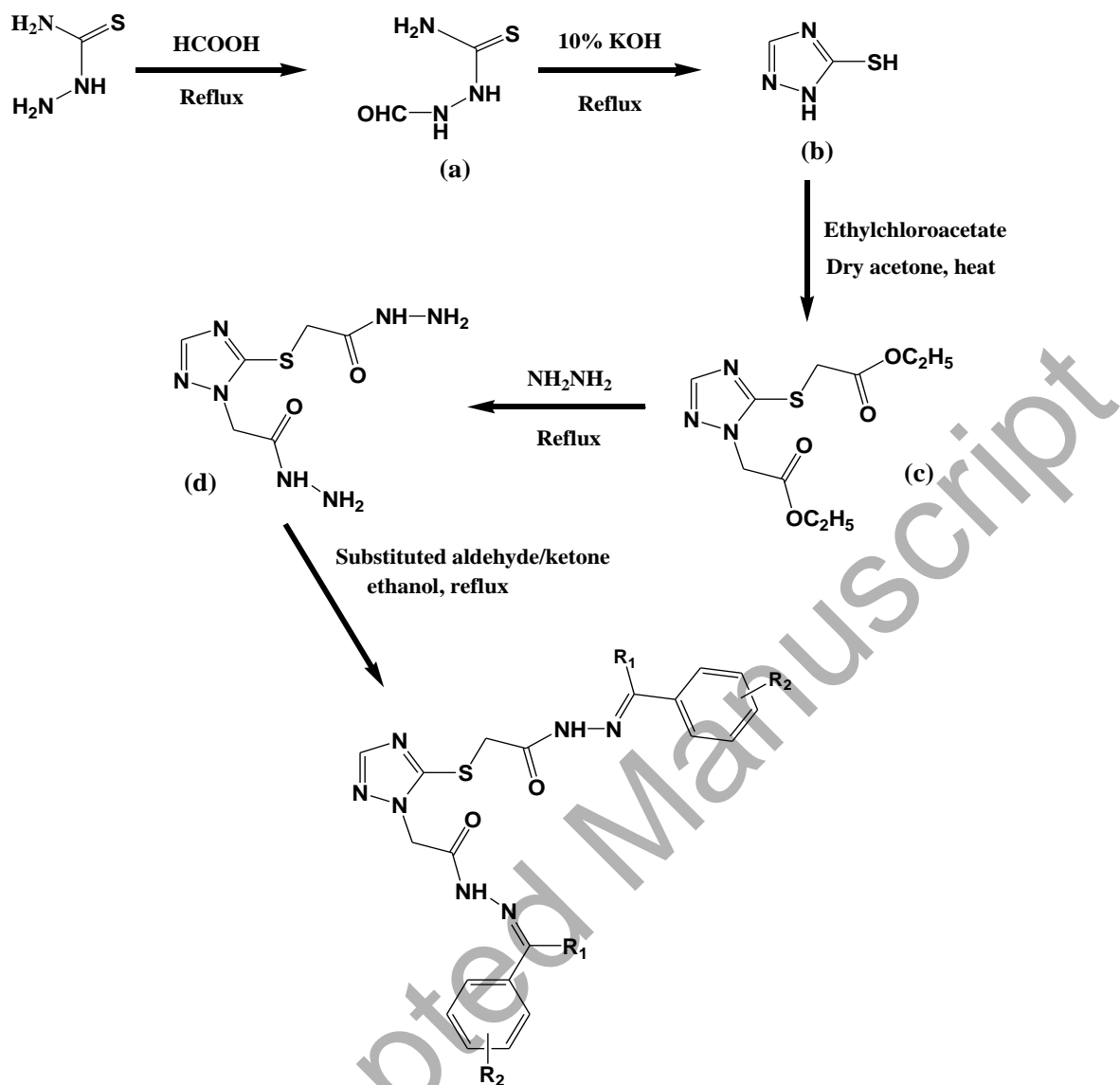
- Morris, G. M., Goodsell, D. S., Halliday, D. S., Huey, R., Hart, W. E., Belew, R. K., & Olson, A. J. (1998). Automated Docking Using a Lamarckian Genetic Algorithm. *J Comput Chem* 19, 1639-1662
- Mur Blanch, N., Chabot, G. G., Quentin, L., Scherman, D., Bourg, S., & Dauzonne, D. (2012). In vitro and in vivo biological evaluation of new 4,5-disubstituted 1,2,3-triazoles as cis-constrained analogs of combretastatin A4. *Eur J Med Chem*, 54, 22-32. doi: 10.1016/j.ejmech.2012.04.017 S0223-5234(12)00269-3 [pii]
- Oyaizu, M. (1986). Studies on products of browning reaction--antioxidative activities of products of browning reaction prepared from glucosamine. *J. Nutrit*, 44, 307-315
- Pan, X., Cao, X., Li, N., Xu, Y., Wu, Q., Bai, J., . . . Lan, L. (2014). Forsythin inhibits lipopolysaccharide-induced inflammation by suppressing JAK-STAT and p38 MAPK signalings and ROS production. *Inflamm Res*, 63(7), 597-608. doi: 10.1007/s00011-014-0731-7
- Papadopoulou, M. V., Bloomer, W. D., Rosenzweig, H. S., Chatelain, E., Kaiser, M., Wilkinson, S. R., . . . Ioset, J. R. (2012). Novel 3-nitro-1H-1,2,4-triazole-based amides and sulfonamides as potential antitrypanosomal agents. *J Med Chem*, 55(11), 5554-5565. doi: 10.1021/jm300508n
- Paprocka, R., Wiese, M., Eljaszewicz, A., Helmin-Basa, A., Gzella, A., Modzelewska-Banachiewicz, B., & Michalkiewicz, J. (2015). Synthesis and anti-inflammatory activity of new 1,2,4-triazole derivatives. *Bioorg Med Chem Lett*, 25(13), 2664-2667. doi: 10.1016/j.bmcl.2015.04.079 S0960-894X(15)00411-4 [pii]
- Pastor, R. W., Brooks, B. R., & Szabo, A. (1988). An analysis of the accuracy of Langevin and molecular dynamics algorithm *Mol. Phys*, 65(6), 1409-1419
- Pokuri, S., Singla, R. K., Bhat, V. G., & Shenoy, G. G. (2014). Insights on the antioxidant potential of 1, 2, 4-triazoles: synthesis, screening & QSAR studies. *Curr Drug Metab*, 15(4), 389-397. doi: CDM-EPUB-62195 [pii]
- Routray, I., & Ali, S. (2019). Boron inhibits apoptosis in hyperapoptosis condition: Acts by stabilizing the mitochondrial membrane and inhibiting matrix remodeling. *Biochim Biophys Acta Gen Subj*, 1863(1), 144-152. doi: S0304-4165(18)30320-9 [pii] 10.1016/j.bbagen.2018.10.007
- Shahzad, S. A., Yar, M., Khan, Z. A., Shahzadi, L., Naqvi, S. A. R., Mahmood, A., . . . Bajda, M. (2019). Identification of 1,2,4-triazoles as new thymidine phosphorylase inhibitors: Future anti-tumor drugs. *Bioorg Chem*, 85, 209-220. doi: S0045-2068(18)30954-4 [pii] 10.1016/j.bioorg.2019.01.005
- Shinkafi, T. S., Kaushik, A., Mahmood, A., Tiwari, A. K., Alam, M. M., Akhter, M., . . . Ali, S. (2019). Computational prediction and experimental validation of the activator function of C2-beta-D-glucopyranosyl-1,3,6,7-tetrahydroxyxanthone on pancreatic and hepatic hexokinase. *J Biomol Struct Dyn*, 1-12. doi: 10.1080/07391102.2019.1650829
- Temraz, A., & El-Tantawy, W. H. (2008). Characterization of antioxidant activity of extract from *Artemisia vulgaris*. *Pak J Pharm Sci*, 21(4), 321-326
- Teng, P., Liu, H. L., Zhang, L., Feng, L. L., Huai, Y., Deng, Z. S., . . . Li, J. X. (2012). Synthesis and biological evaluation of novel sinomenine derivatives as anti-inflammatory agents.

Eur J Med Chem, 50, 63-74. doi: 10.1016/j.ejmech.2012.01.036 S0223-5234(12)00051-7 [pii]

- Timur, I., Kocyigit, U. M., Dastan, T., Sandal, S., Ceribasi, A. O., Taslimi, P., . . . Ciftci, M. (2018). In vitro cytotoxic and in vivo antitumoral activities of some aminomethyl derivatives of 2,4-dihydro-3H-1,2,4-triazole-3-thiones-Evaluation of their acetylcholinesterase and carbonic anhydrase enzymes inhibition profiles. *J Biochem Mol Toxicol*, e22239. doi: 10.1002/jbt.22239
- Uberuaga, B. P., Anghel, M., & Voter, A. F. (2004). Synchronization of trajectories in canonical molecular-dynamics simulations: observation, explanation, and exploitation. *J Chem Phys*, 120(14), 6363-6374. doi: 10.1063/1.1667473
- Wani, M. Y., Bhat, A. R., Azam, A., & Athar, F. (2013). Nitroimidazolyl hydrazones are better amoebicides than their cyclized 1,3,4-oxadiazoline analogues: In vitro studies and Lipophilic efficiency analysis. *Eur J Med Chem*, 64, 190-199. doi: 10.1016/j.ejmech.2013.03.034 S0223-5234(13)00194-3 [pii]
- Winter, C. A., Risley, E. A., & Nuss, G. W. (1962). Carrageenin-induced edema in hind paw of the rat as an assay for antiinflammatory drugs. *Proc Soc Exp Biol Med*, 111, 544-547
- Xiao, Z. P., Wang, X. D., Wang, P. F., Zhou, Y., Zhang, J. W., Zhang, L., . . . Zhu, H. L. (2014). Design, synthesis, and evaluation of novel fluoroquinolone-flavonoid hybrids as potent antibiotics against drug-resistant microorganisms. *Eur J Med Chem*, 80, 92-100. doi: 10.1016/j.ejmech.2014.04.037 S0223-5234(14)00358-4 [pii]
- Y. L. Fan, X. K., M. Li. . J. (2018). Coumarin-triazole hybrids and their biological activities. *Heterocyclic Chem.*, 55, 791-802
- Zhang, H. Z., Damu, G. L. V., Cai, G. X., & Zhou, C. H. (2014). Current developments in the syntheses of 1,2,4-triazole compounds. *Current Organic Chemistry*, 18, 359-406
- Zhang, J., Wang, S., Ba, Y., & Xu, Z. (2019). 1,2,4-Triazole-quinoline/quinolone hybrids as potential anti-bacterial agents. *Eur J Med Chem*, 174, 1-8. doi: S0223-5234(19)30348-4 [pii] 10.1016/j.ejmech.2019.04.033
- Zhang, Q., Peng, Y., Wang, X. I., Keenan, S. M., Arora, S., & Welsh, W. J. (2007). Highly potent triazole-based tubulin polymerization inhibitors. *J Med Chem*, 50(4), 749-754. doi: 10.1021/jm061142s
- Zhang, S., Xu, Z., Gao, C., Ren, Q. C., Chang, L., Lv, Z. S., & Feng, L. S. (2017). Triazole derivatives and their anti-tubercular activity. *Eur J Med Chem*, 138, 501-513. doi: S0223-5234(17)30505-6 [pii] 10.1016/j.ejmech.2017.06.051



Workflow 1: Flow chart depicting stepwise analysis of synthetic derivatives to shortlist the compound with maximum anti-inflammatory activity and elucidation of its mechanisms of action.



Scheme 1: An outline of the synthetic scheme depicting the new synthetic route for the synthesis of 1,2,4-triazole and its derivatives.

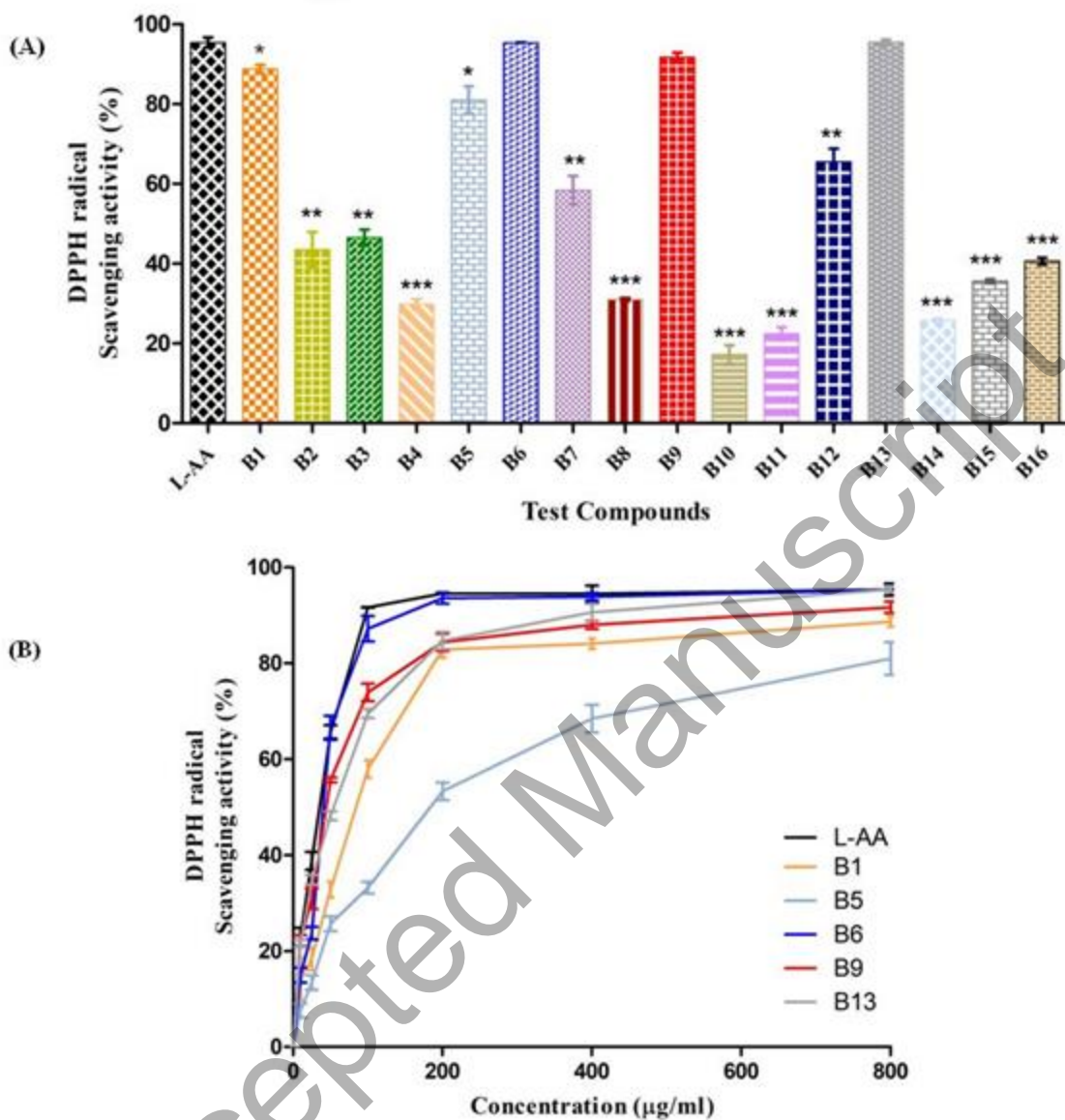


Fig.1: Free radical inhibition activity of 1,2,4-triazole and its derivatives. (A) Free radical scavenging activity of 1,2,4-triazole and its derivatives (B1-B16) as determined by the DPPH assay. (B) Compounds with 80-90% free radical inhibition were further investigated and five compounds B1, B5, B6, B9, and B13 were identified as a potent radical scavengers showing highest DPPH radical scavenging activity comparable to the standard antioxidant, L-AA. L-AA: L-ascorbic acid. $p^* < 0.05$, $p^{**} < 0.01$, $p^{***} < 0.001$.

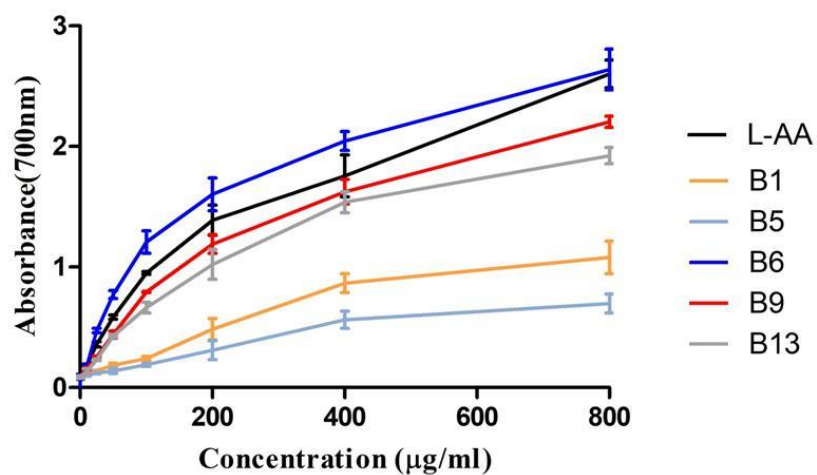


Fig.2: TRC of 1,2,4-triazole and its derivatives. TRC of B6 was highest, suggesting it to be a strong reductant compared with L-AA (L-ascorbic acid). TRC: Total reduction capability.

Accepted Manuscript

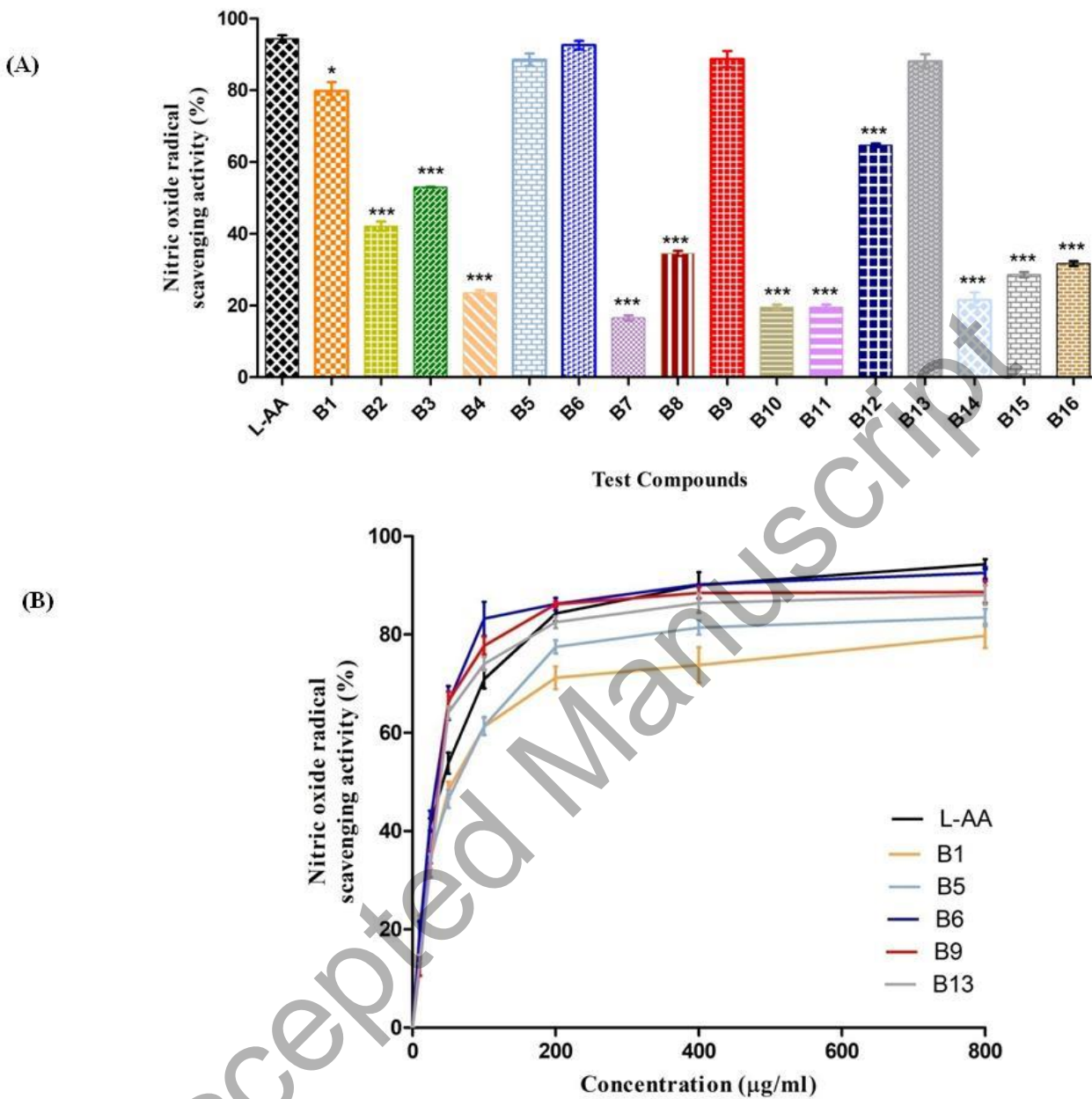


Fig.3: Nitric oxide radical scavenging activity of 1,2,4-triazole derivatives. (A) Nitric oxide radical scavenging activity of the standard (L-AA) and various derivatives (B1-B16). (B) Nitric oxide scavenging activity of B1, B5, B6, B9 and B13. The activity of these compounds was 80-90% when compared with the standard. L-AA: L-ascorbic acid. $p^* < 0.05$, $p^{**} < 0.01$, $p^{***} < 0.001$.

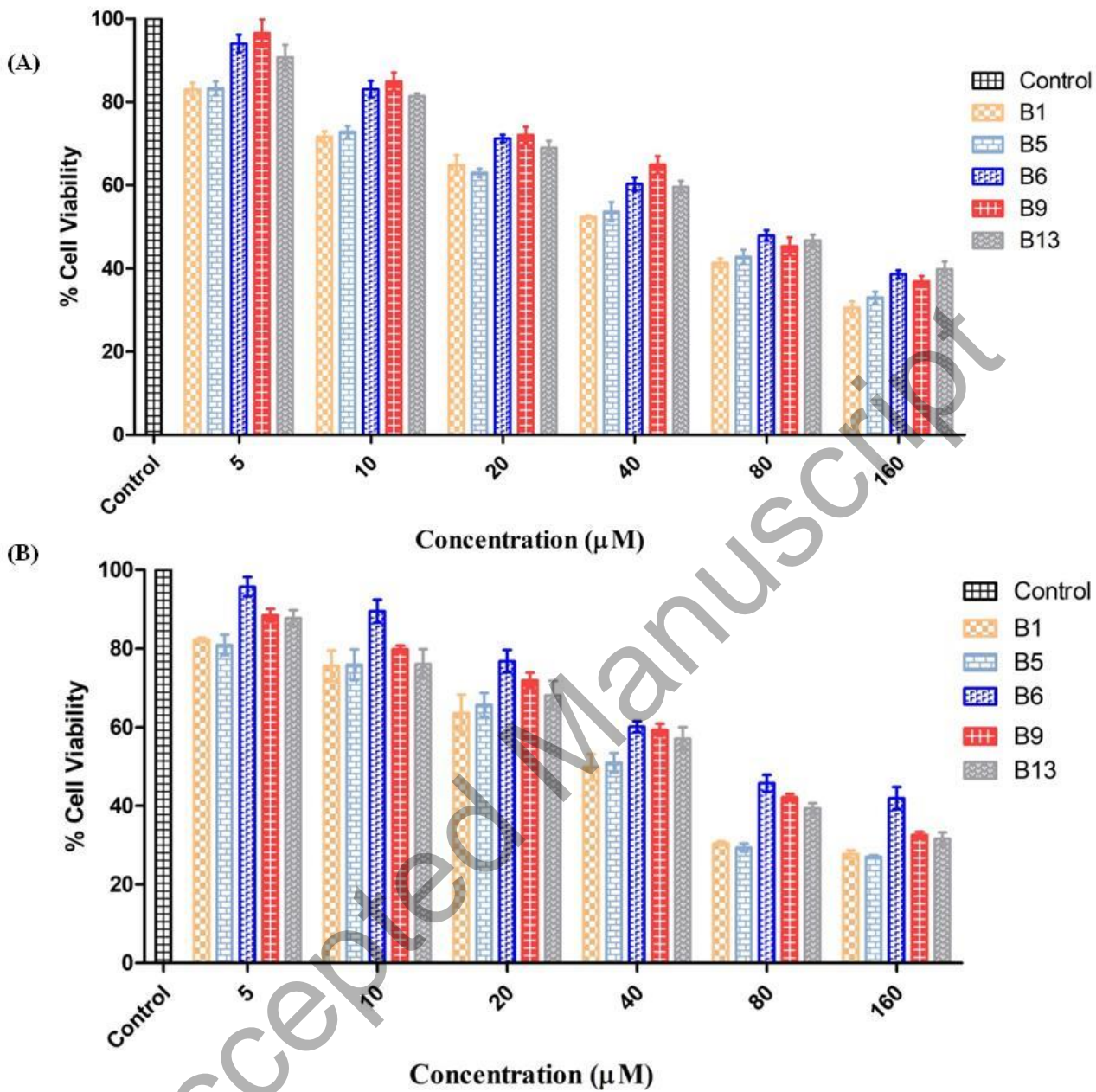


Fig.4: Cell viability assay. The cell viability was measured in (A) RAW 264.7, and (B) J774.1 cell. Each value represents Mean \pm SD (n=3).

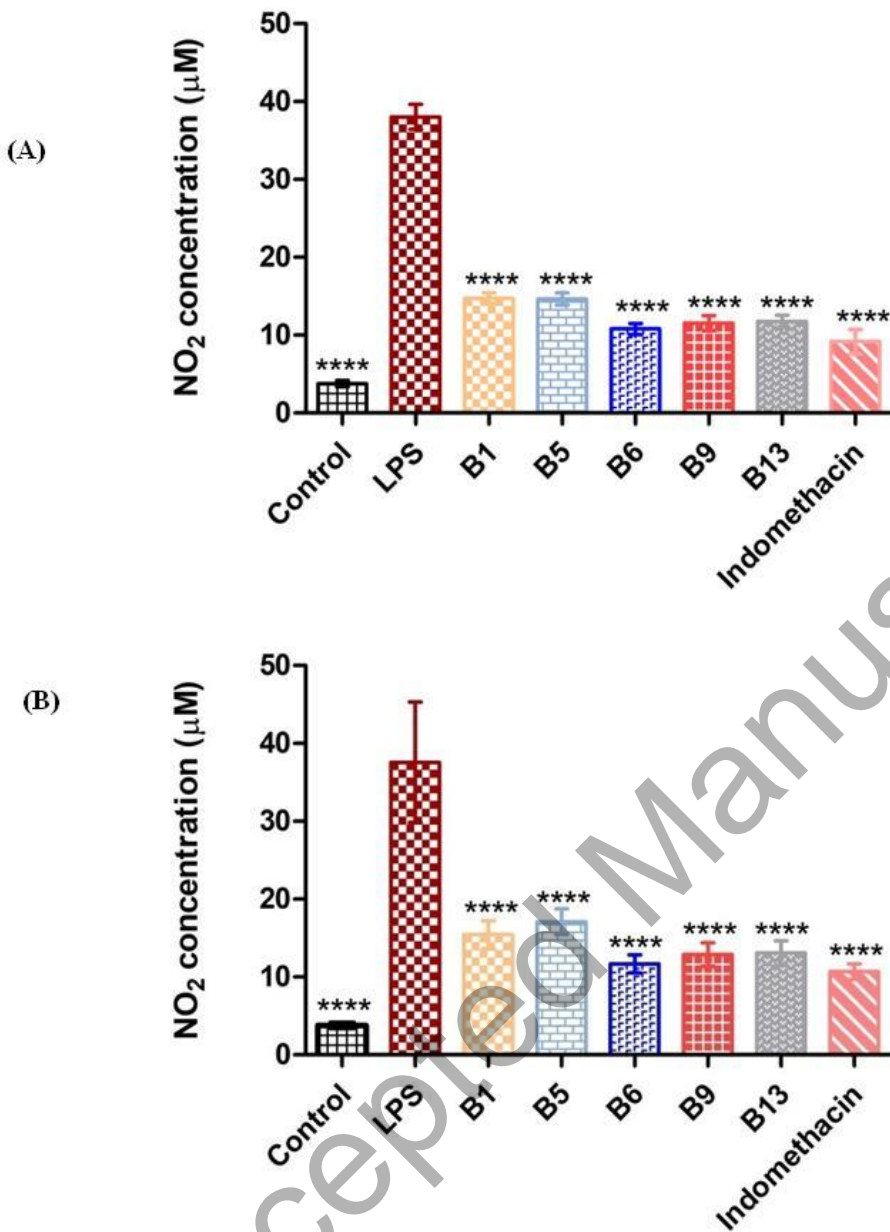


Fig.5: Nitrite production by the LPS-stimulated macrophage cells. The nitrite level was significantly lowered by B6 in both (A) RAW 264.7, and (B) J774.1A cells. Each value represents Mean \pm SD (n=3). **** $p < 0.0001$, when compared with the LPS-stimulated untreated cells.

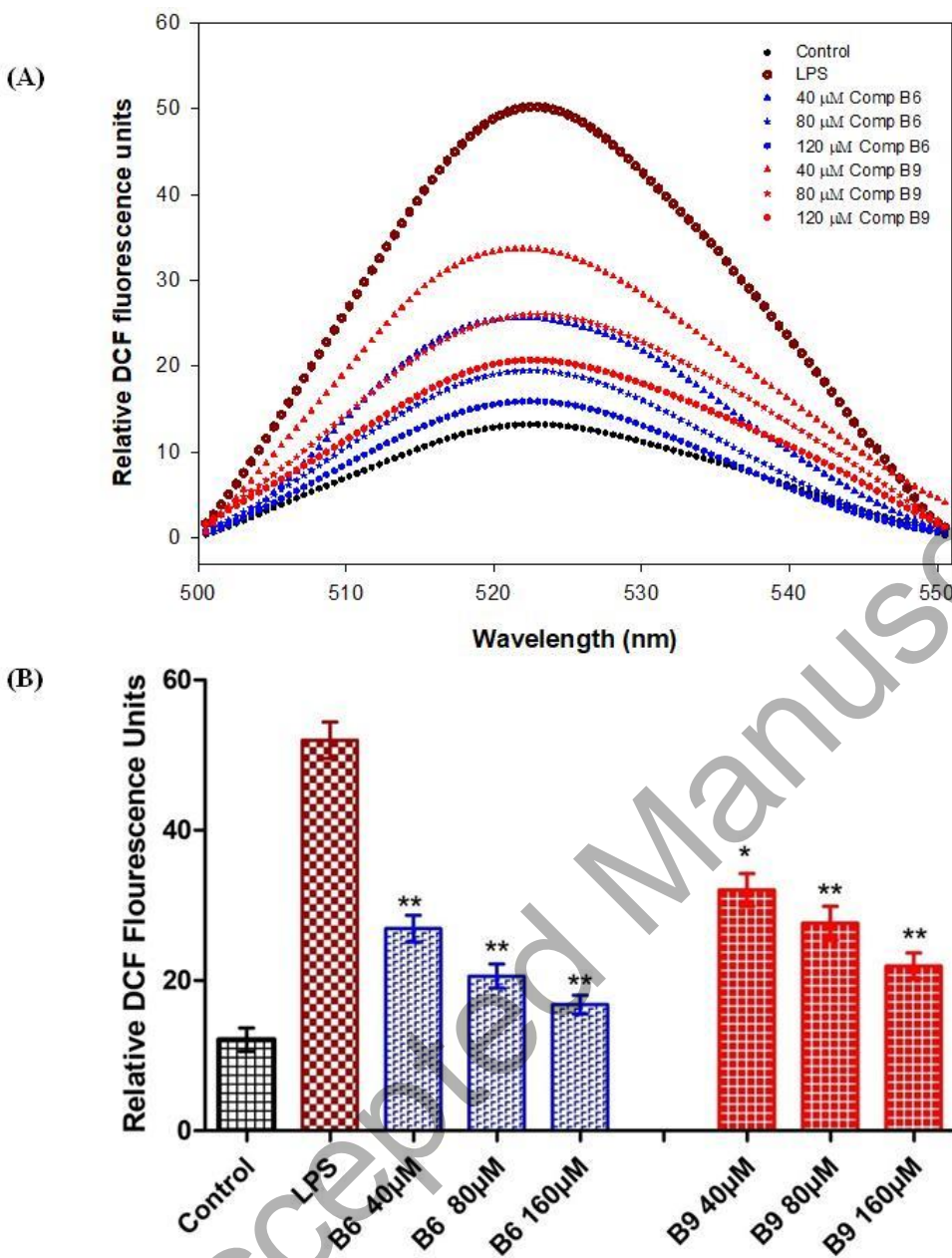


Fig.6: DCFH-DA assay in LPS-stimulated J774.1A cell. (A) The fluorescence emission spectrum of J774.1A and DCF probe, obtained after treatment with increasing concentration (40, 80, 160μM) of B6 and B9. (B) Bar diagram showing relative DCF fluorescence intensity in triplicate (Mean ± SD) with B6 and B9 showing a significant decrease in ROS level, indicating intracellular antioxidant activity of the compounds. Statistical analysis was done by the *t*-test for unpaired samples. Values were significantly different when compared with the LPS-treated group (* $p < 0.5$, ** $p < 0.01$). DCFH-DA: Dichloro-dihydro-fluorescein diacetate.

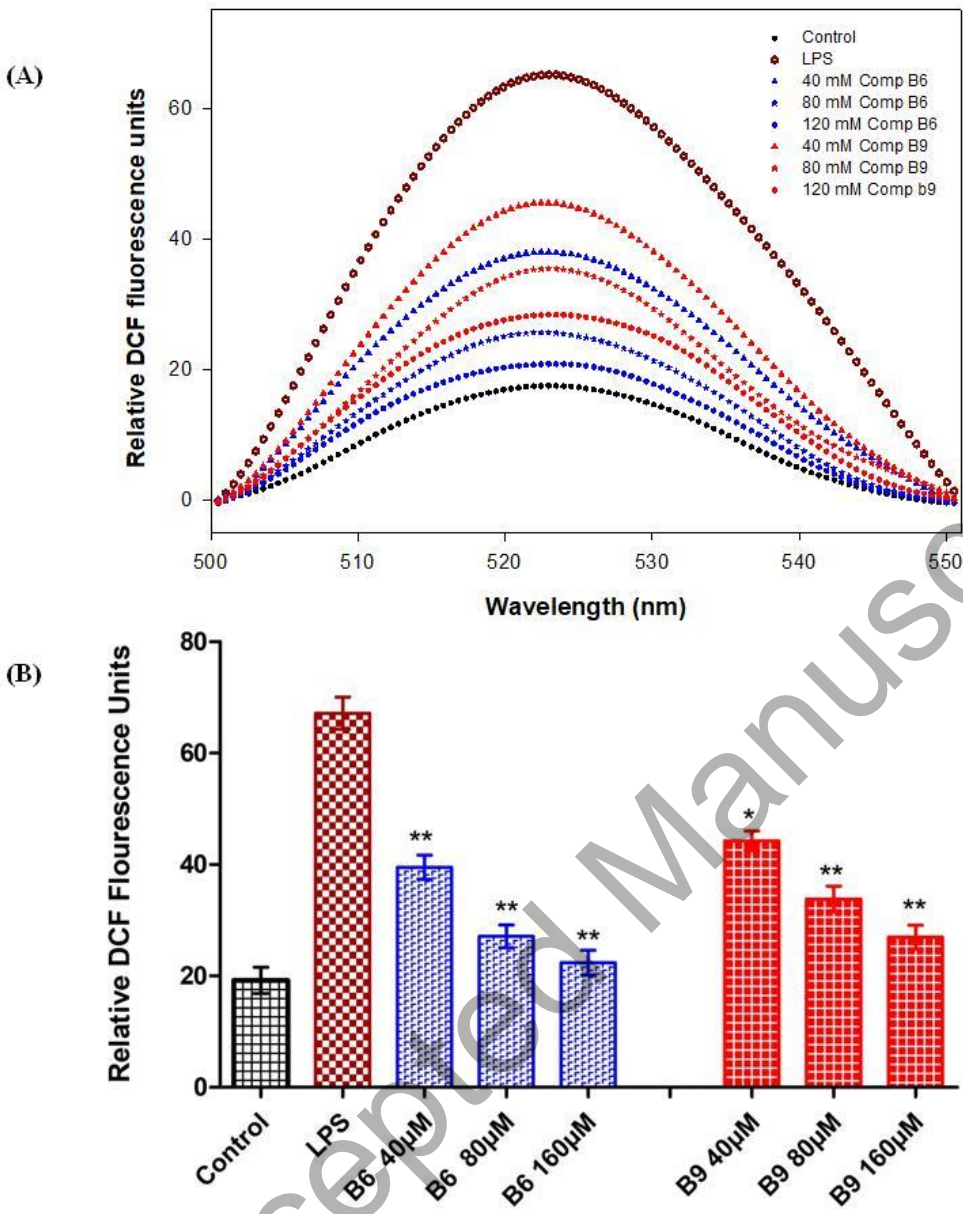


Fig.7: DCFH-DA in LPS-stimulated RAW 264.7 cells. (A) The fluorescence emission spectrum of RAW 264.7 and DCF probe in cultures treated with 40, 80, or 160µM of B6 and B9, and (B) Bar diagram representation of relative DCF fluorescence intensity (Mean ± SD, n=3) of respective (B6, B9) groups, showing a significant reduction in ROS production, suggesting an intracellular antioxidant activity of the derivatives. * $p < 0.05$ and ** $p < 0.01$, when compared with the LPS group. LPS: Lipopolysaccharide.

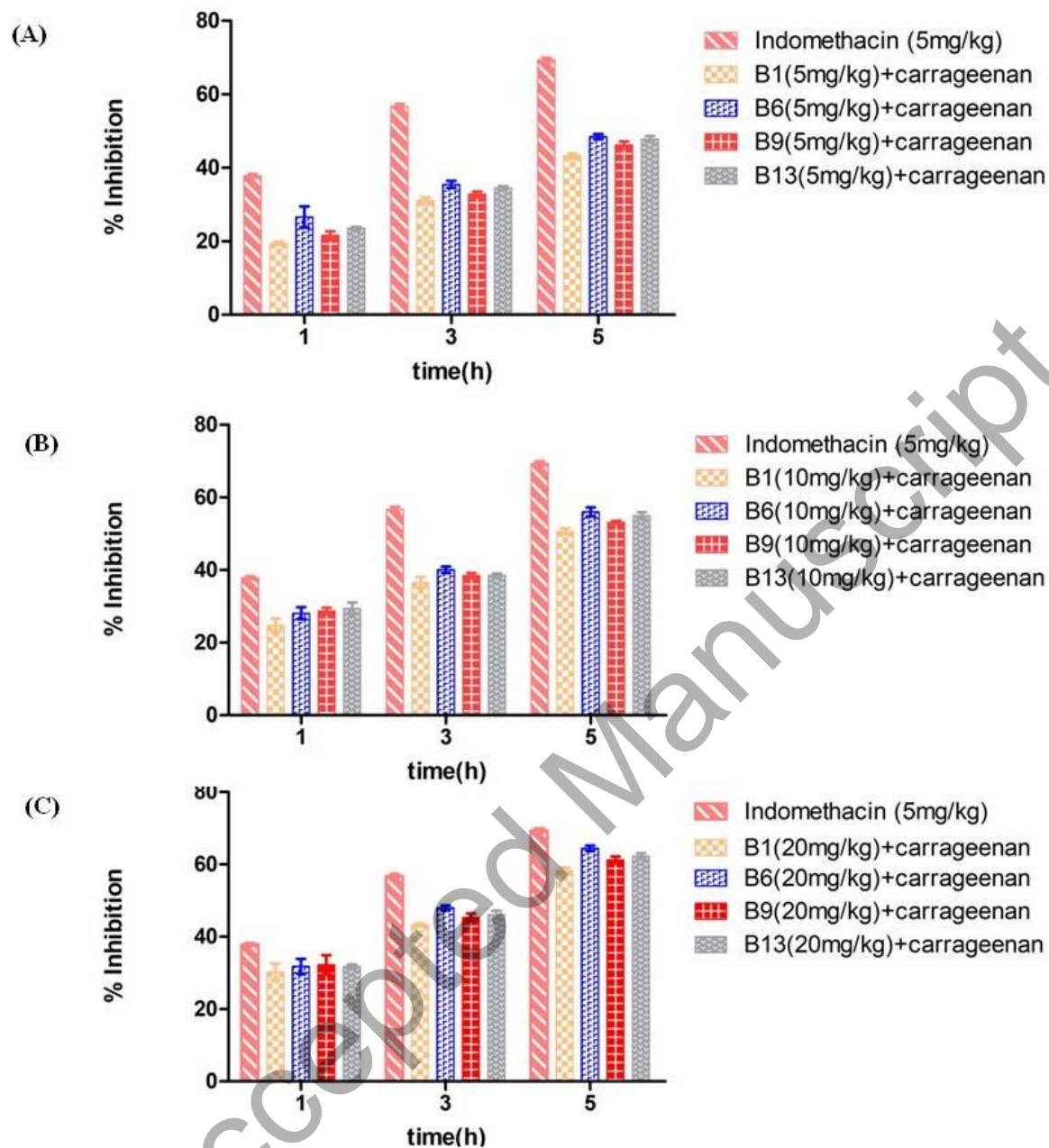


Fig.8: Effect of B6 and other derivatives on carrageenan-induced inflammation in rat. When compared with the untreated control group and standard drug indomethacin, B6 showed a significant reduction in inflammation ($*p < 0.05$) at (A) 5, (B) 10, and (C) 20mg/kg body weight. Each value represents the Mean \pm SD of six rats in each group.

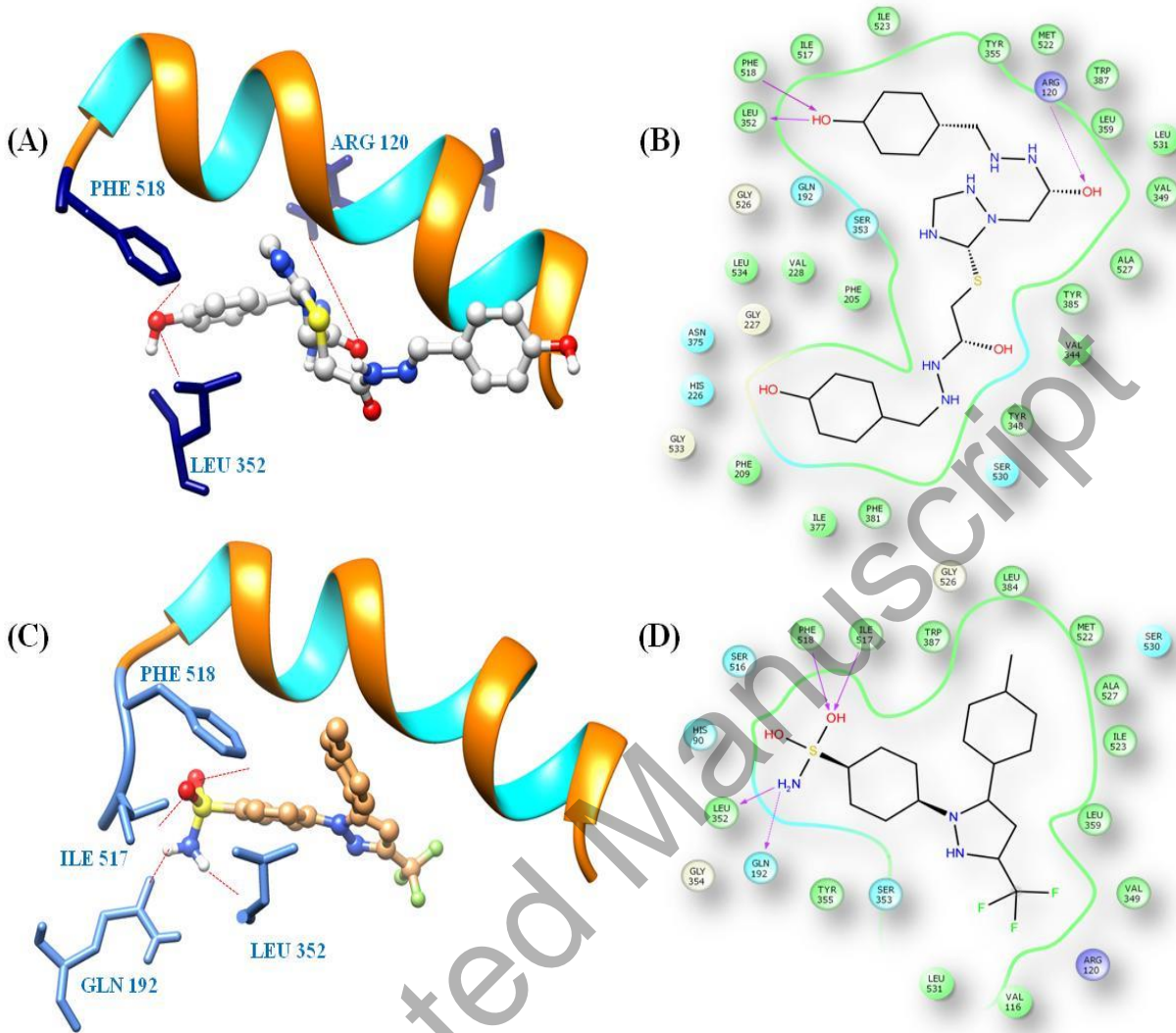


Fig.9: Molecular docking of B6 with COX-1 against celecoxib. (A) 2D binding pattern of B6 (light gray) in celecoxib binding site of COX-1 (important residues highlighted in navy blue), and (B) LigPlot of B6 in the COX-1 binding pocket. (C) The binding mode of celecoxib (brown) in COX-1 active site (important residues tinted with cornflower blue). (D) LigPlot image of celecoxib.

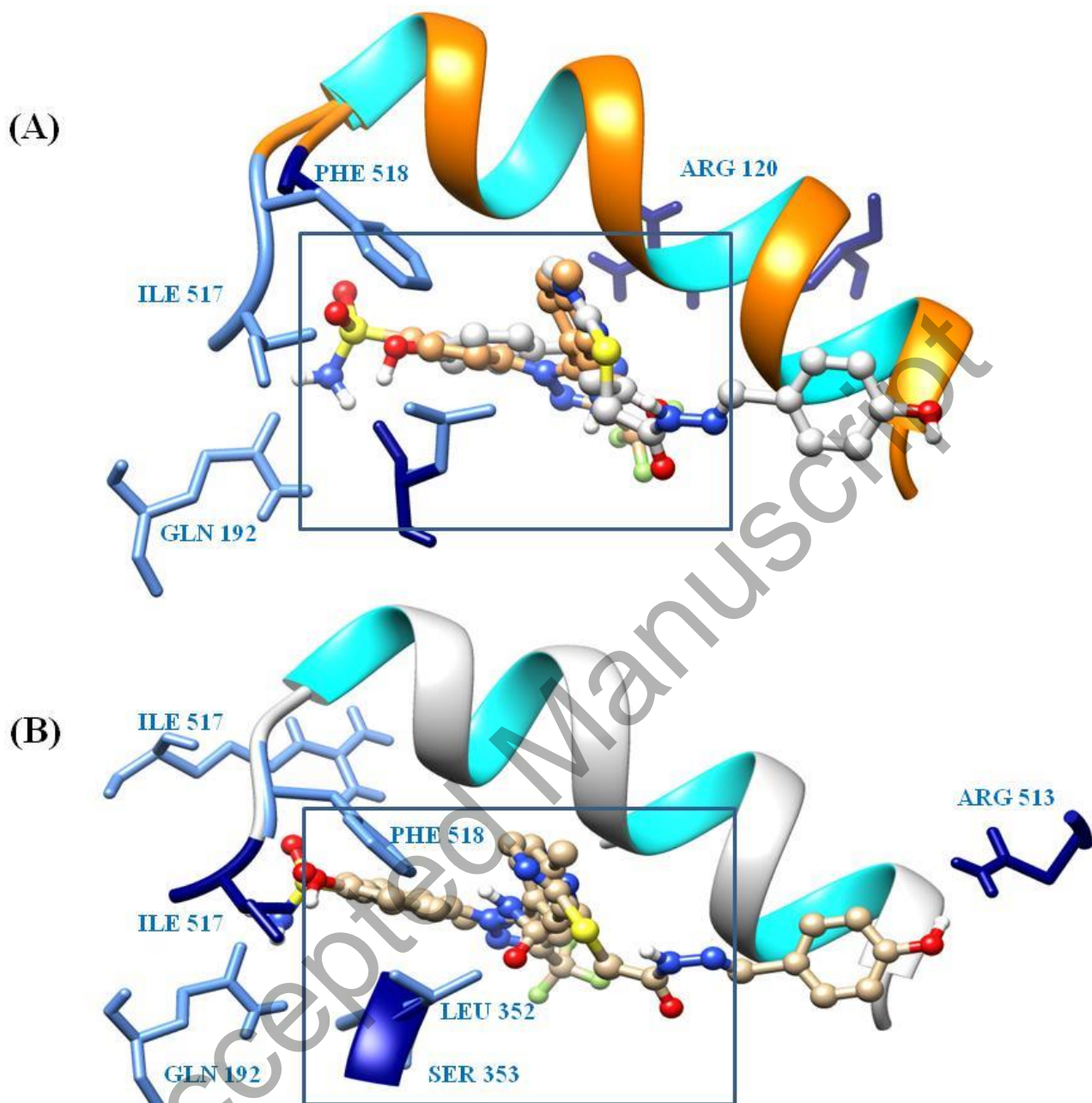


Fig.11: Superimposition of B6 (light gray) with celecoxib (brown) in the catalytic domain of (A) COX-1, and (B) COX-2.

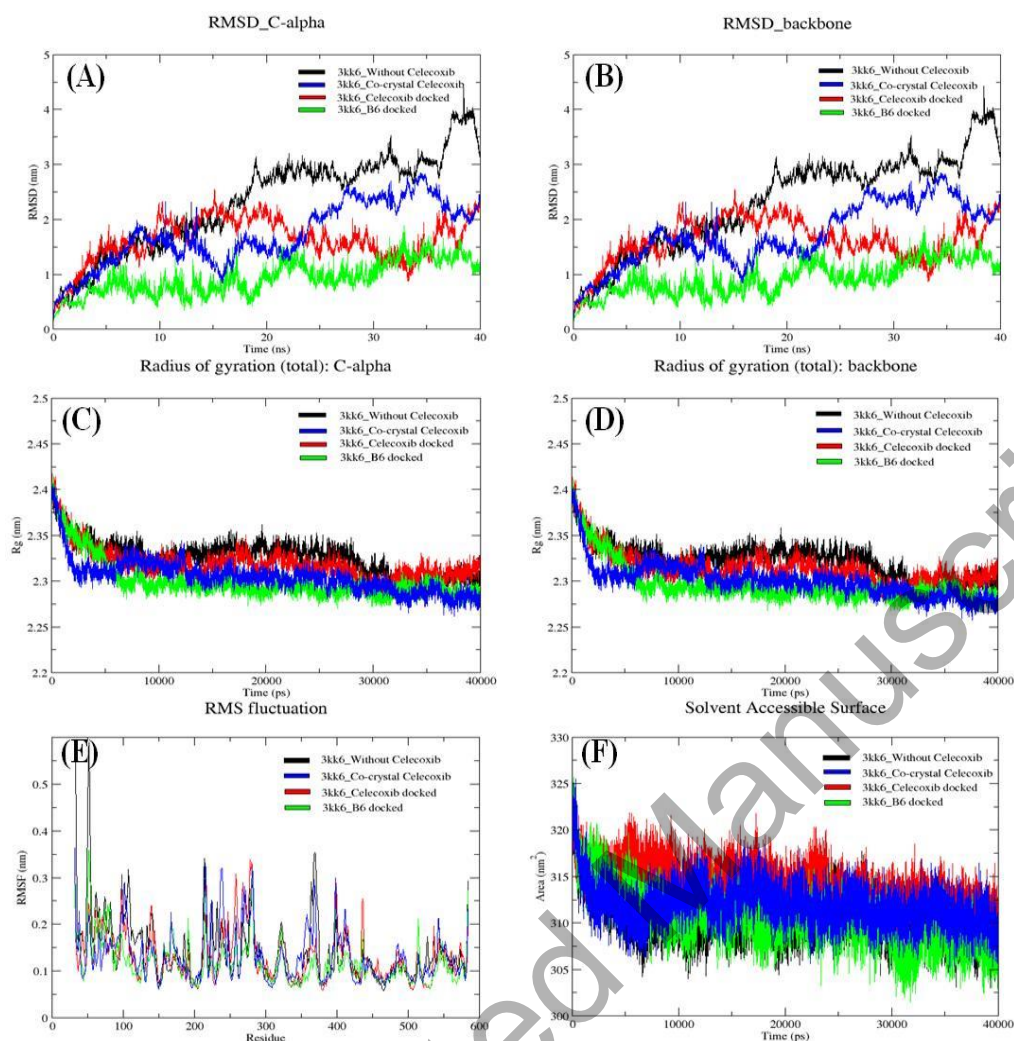


Fig.12: MD simulation of B6 with COX-1. (A) Root-mean square deviation (RMSD) plot of all C- α atoms for COX-1 (PDB ID:3kk6) without celecoxib (black), co-crystal celecoxib (blue), complex with docked celecoxib (red), and complex with docked B6 (green) (B) Backbone RMSD plot of COX-1 without celecoxib (black), co-crystal celecoxib (blue), complex with docked celecoxib (red), and complex with docked compound B6 (green) (C) Time evolution of the radius of gyration (Rg) for COX-1 without celecoxib (black), co-crystal celecoxib (blue), complex with docked celecoxib (red), and complex with docked compound B6 (green) (D) Backbone Rg for COX-1 without celecoxib (black), co-crystal celecoxib (blue), complex with docked celecoxib (red), and complex with docked compound B6 (green) (E) Time-average Root mean square fluctuations (RMSF) plot of COX-1 without celecoxib (black), co-crystal celecoxib (blue), complex with docked celecoxib (red), and B6 (green) (F) Time evolution plot of the solvent accessible surface area (SASA) for each residue of COX-1 without celecoxib (black), co-crystal celecoxib (blue), complex with docked celecoxib (red), and compound B6 (green) in water at 300 k during 40 ns MD simulation.

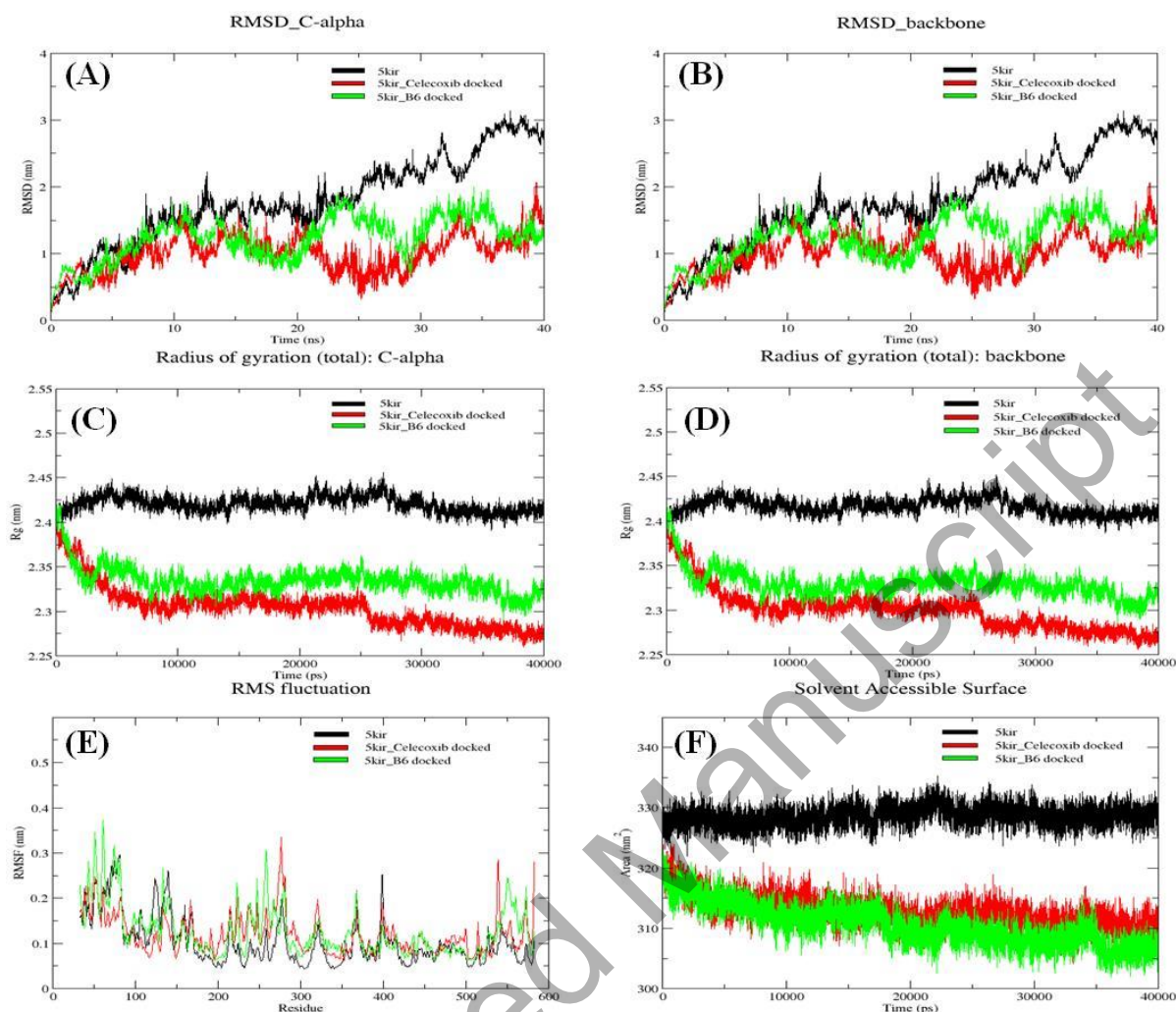


Fig.13: MD simulation of B6-COX-2 complex. (A) Root-mean square deviation (RMSD) plot of all C- α atoms for COX-2 (PDB ID: 3kk6) without celecoxib (black), complex with docked celecoxib (red), and complex with docked derivative B6 (green) (B) Backbone RMSD plot of COX-2 without celecoxib (black), complex with docked celecoxib (red), and complex with docked compound B6 (green) (C) Time evolution of the radius of gyration (Rg) for COX-2 without celecoxib (black), complex with docked celecoxib (red), and complex with docked compound B6 (green) (D) Backbone Rg for COX-2 without celecoxib (black), complex with docked celecoxib (red), and complex with docked B6 (green) (E) Time-average RMSF plot of COX-2 without celecoxib (black), complex with docked celecoxib (red), and B6 (green) (F) Time evolution plot of the solvent accessible surface area (SASA) for each residue of COX-2 without celecoxib (black), complex with docked celecoxib (red), and compound B6 (green) in water at 300 k in a 40 ns run.

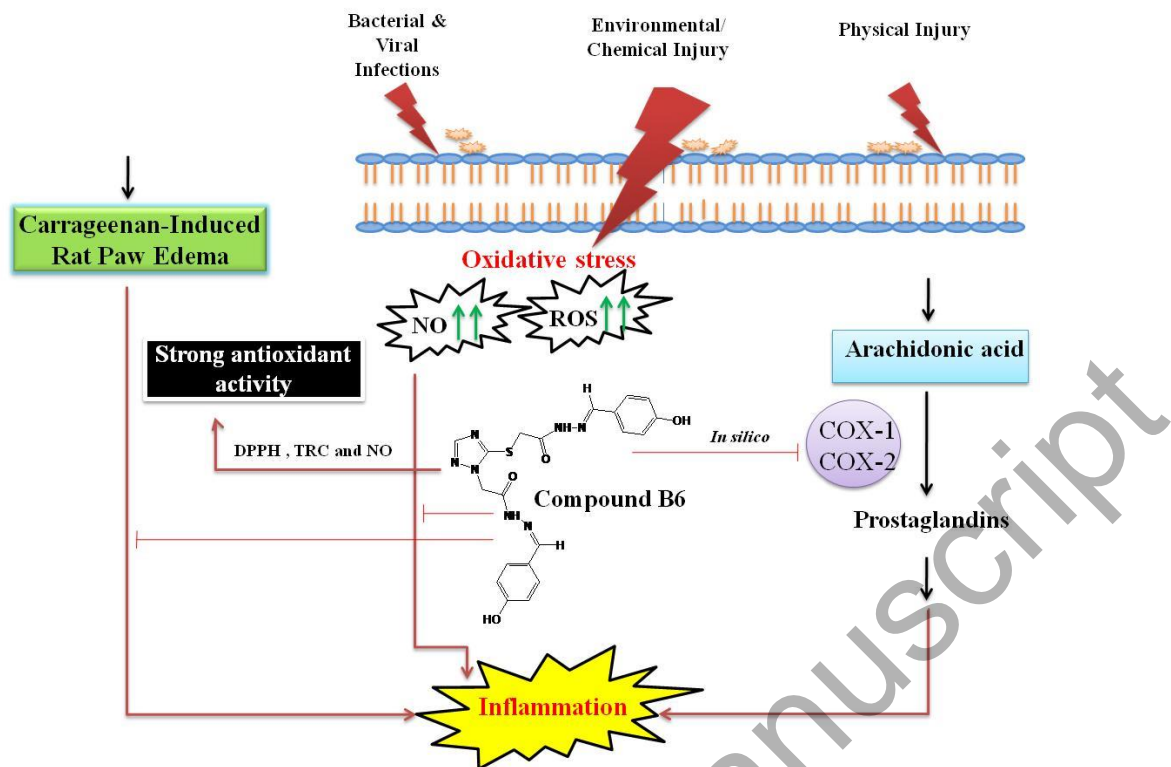


Fig.14: Illustrated pathway showing B6 and its role in blocking inflammation.

Table 1: Substituted R groups of all sixteen newly synthesized derivatives of 1,2,4-triazole

<i>Compound Name</i>	<i>R₁</i>	<i>R₂</i>
B1	<i>H</i>	<i>2,5- OCH₃</i>
B2	<i>H</i>	<i>4-OCH₃</i>
B3	<i>H</i>	<i>3,4- OCH₃</i>
B4	<i>H</i>	<i>4-CH₃</i>
B5	<i>H</i>	<i>2-NO₂</i>
B6	<i>H</i>	<i>4-OH</i>
B7	<i>H</i>	<i>2-OC₂H₅</i>
B8	<i>H</i>	<i>4-OC₂H₅</i>
B9	<i>CH₃</i>	<i>2,4-OH</i>
B10	<i>H</i>	<i>3- OCH₃, 4-OH</i>
B11	<i>CH₃</i>	<i>2,5- OCH₃</i>
B12	<i>CH₃</i>	<i>3,4- OCH₃</i>
B13	<i>CH₃</i>	<i>4-CH₃</i>
B14	<i>CH₃</i>	<i>4-OCH₃</i>
B15	<i>H</i>	<i>3-NO₂</i>
B16	<i>H</i>	<i>4-Cl</i>

Accepted Manuscript

Table 2: Antioxidant and nitric oxide radical scavenging activity of B1, B5, B6, B9 and B13 and their IC₅₀

Compound	Concentration (µg/ml)	Antioxidant activity		Nitric oxide	
		% Inhibition	IC ₅₀ (µg/ml)	% Inhibition	IC ₅₀ (µg/ml)
B1	800µg/ml	88.69 ± 1.05	82.88 ± 1.732	79.75 ± 2.46	57.29±1.73
B5		80.98 ± 3.40	179.69 ± 1.05	83.49 ± 1.72	60.49 ± 1.72
B6		95.31 ± 0.12	38.79 ± 1.88	92.55 ± 1.18	32.40 ± 0.62
B9		91.67 ± 1.20	43.30 ± 1.79	88.65 ± 2.22	36.33 ± 1.71
B13		95.45 ± 0.64	55.66 ± 0.53	88.03 ± 1.94	37.39 ± 1.94
LAA		95.36 ± 1.24	35.58 ± 1.52	94.31 ± 0.99	43.46 ± 1.3

The antioxidant activity was measured by DPPH, 2,2-diphenyl-1-picryl-hydrazyl-hydrate, assay. All values are shown in Mean ± SD.

IC₅₀: Inhibitory concentration, µg/ml. LAA: L-Ascorbic acid.

Accepted Manuscript

Table 3: IC₅₀ of test compounds in RAW 264.7 and J774.1 culture

Compound	R ₁	R ₂	IC ₅₀ (μM)	
			RAW 264.7	J774.1
			B1	<i>H</i>
B5	<i>H</i>	<i>o-NO₂</i>	49.5±1.3	41.5±2.0
B6	<i>H</i>	<i>p-OH</i>	69±1.5	62±1.4
B9	<i>CH₃</i>	<i>o, p-OH</i>	66±2.0	57±1.6
B13	<i>CH₃</i>	<i>p-CH₃</i>	65±1.7	52.5±1.3

IC₅₀ was measured by the MTT assay. Each value represents Mean ± SD (n=3).

Table 4: Effect of derivatives on LPS-stimulated synthesis of nitric oxide in RAW 264.7 and J774.1A cells

Compound	R ₁	R ₂	RAW 264.7		J774.1A	
			NO synthesis, μ M	% Inhibition	NO synthesis, μ M	% Inhibition
Control	-	-	3.79 \pm 0.39	-	3.79 \pm 0.39	-
LPS	-	-	38.04 \pm 1.61	-	37.57 \pm 7.73	-
B1	H	o,m-OCH ₃	14.75 \pm 0.68	70.11 \pm 1.74	15.43 \pm 1.81	66.79 \pm 4.64
B5	H	o-NO ₂	14.66 \pm 0.78	70.32 \pm 1.99	17.08 \pm 1.67	62.53 \pm 4.26
B6	H	p-OH	10.81 \pm 0.71	80.10 \pm 1.84	11.68 \pm 1.17	76.34 \pm 2.99
B9	CH ₃	o, p-OH	11.56 \pm 0.98	78.17 \pm 2.47	12.89 \pm 1.51	73.25 \pm 3.87
B13	CH ₃	p-CH ₃	11.77 \pm 0.80	77.66 \pm 2.03	13.09 \pm 1.57	72.77 \pm 4.02
IDM	-	-	9.19 \pm 1.57	84.18 \pm 3.99	10.7 \pm 0.99	78.89 \pm 2.54

IDM: indomethacin, used as standard drug. Each value represents Mean \pm SD (n=3).

Accepted Manuscript

Table 5: Anti-inflammatory effect of selected synthetic derivatives in rat model

Groups	Dose (mg/kg)	Paw edema thickness in mm (values in bracket indicate % inhibition)			Potency at 5 h, Relative to IDM
		1 h	3 h	5 h	
Control	-	1.54±0.026	2.687±0.0075	3.69±0.052	-
IDM	5	0.957±0.007	1.163±0.017	1.131±0.023	1.00
		(37.85%)	(56.72%)	(69.34%)	
B6	5	1.130±0.044*	1.733±0.025*	1.901±0.025*	0.69
		(26.62%)	(35.5%)	(48.48%)	
	10	1.107±0.025*	1.610±0.024*	1.623±0.045*	0.80
		(28.11%)	(40.08%)	(56.01%)	
	20	1.050±0.032*	1.398±0.018*	1.312±0.026*	0.92
		(31.81%)	(47.97%)	(64.44%)	
B1	5	1.24±0.006*	1.846±0.016*	2.093±0.023*	0.62
		(19.48%)	(31.29%)	(43.27%)	
	10	1.159±0.029*	1.694±0.04*	1.821±0.031*	0.73
		(24.74%)	(36.95%)	(50.65%)	
	20	1.073±0.035*	1.524±0.01*	1.535±0.029*	0.84
		(30.32%)	(43.28%)	(58.4%)	
B9	5	1.207±0.017*	1.805±0.021*	1.984±0.034*	0.66
		(21.62%)	(32.84%)	(46.23%)	
	10	1.097±0.013*	1.653±0.019*	1.729±0.015*	0.76
		(28.76%)	(38.48%)	(53.14%)	
	20	1.043±0.04*	1.469±0.029*	1.431±0.035*	0.88
		(32.27%)	(45.32%)	(61.21%)	
B13	5	1.177±0.005*	1.758±0.012*	1.924±0.028*	0.69
		(23.57%)	(34.57%)	(47.85%)	
	10	1.087±0.025*	1.651±0.013*	1.661±0.035*	0.79
		(29.41%)	(38.55%)	(54.98%)	
	20	1.051±0.009*	1.448±0.028*	1.392±0.030*	0.89
		(31.75%)	(46.11%)	(62.27%)	

Each value represents Mean ± SEM (n=6).

The level of significance was * $p < 0.05$, when compared with indomethacin (IDM).

Table 6: Binding free energies of B1, B5, B6, B9 and B13 with COX-1 and COX-2

Complex	ΔG , kcal/mol	H bond	Hydrophobic interaction	Polar interaction	Positive charge & glycine interaction
B1-COX 1	-8.0	R 120	P86, I89, L93, L115, V116, V119, L344, Y348, V349, L352, Y355 , L359, F381, L384, Y385, W387, F518, M522, I523, A527, L531	S353, S530	G526
B5-COX 1	-8.8	R 120	I89, L93, L112, L115, V116, V119, V349, Y355 , L357, L359, F381, L384, Y385, W387, F518, M522, I523, A527, L531	S353, S530	G526
B6-COX 1	-10.5	R120, L352, F518	F205, F209, V228, V344, Y348, V349, Y355 , L359, I377, F381, Y385, W387, I517, M522, I523, A527, L531, L534	Q192, H226, S353, N375, S530	G227, G526 , G533
B9-COX 1	-8.7	M 522	I89, L93, V116, V119, Y348, V349 , L352, Y355 , F381, L384, Y385, W387, F518, M522, I523, A527, L531	S353, S530	R120, G526
B13-COX 1	-7.6	#	P86, I89, L93, V116, V119, Y348, V349 , L352, Y355 , F381, L384, Y385, W387, F518, M522, I523, A527, L531	S353, S530	R120, G526
Celecoxib-COX 1	-10.7	Q192, L352, F518 , I517	V116, V349, Y355 , L359, L384, W387, M522, I523, A527, L531	H90, S353, S516, S530	R120, G354, G526
B1-COX 2	-7.8	R120	P86, V89, L93, Y115, V116, Y348, V349, L352, Y355 , I359, F381, L384, Y385, W387, F518, M522, I523, A527, L531	S353, S530	G526
B5-COX 2	-8.3	Y385	P86, V89, L93, Y115, V116, L123, Y348, V349, L352, Y355 , I359, L384, W387, F518, M522, I523, A527, L531	S119, S353, S530	R120, G526
B6-COX 2	-11.2	Q192, L352 , I517, N375	F205, F209, V228, V344, Y348, V349, Y355 , I377, F381, Y385, W387, A516, F518, M522, I523, A527, F529, L534	H90, H226, S353, S530	R513, G227, G526 , G533
B9-COX 2	-8.9	S530	V89, L93, Y115, V116, L123, V349, L352, Y355 , I359, F381, L384, Y385, W387, F470, M471 ,	S119, S353	L83, R120, G526

			F518 , M522 , I523, A527 , L531		
B13-COX 2	-8.0	#	V116, F205, F209, V228, V344, Y348, V349 , L352 , Y355 , I359, I377, L385, Y385, W387 , F518 , M522 , I523, A527 , F529, L531, L534	H90, T206, H226, S353 , N375, S530	R120, R513, G227, G526 , G533
Celecoxib-COX 2	-11.8	Q192, L352 , S353 , R513, F518	V116, V349 , Y355 , I359, L384, W387 , A516, I517, M522 , V523, A527 , L531	H90, S530	R120, G354, G526

#Indicate no hydrogen bond formation with any of the residues of the target protein.

Numbers in bold (red color) highlights the common binding residues in standard drug and synthesized derivatives for COX-1, whereas the bold and underlined values (in blue) represent the same for COX-2.

Accepted Manuscript